UNIVERSITÄT GREIFSWALD
Wissen lockt. Seit 1456

Spin-polarized effects in superconducting hybrid structures

A thesis submitted for the degree of

Bachelor of Science

presented by
Leo Kollwitz
born August 3, 2000
in Neustrelitz

Primary reviewer
Professor Dr. Matthias Eschrig

Secondary reviewer
Dr. Anna Posazhennikova

Greifswald
July 7, 2022

Spin-polarized effects in superconducting hybrid structures

Leo Kollwitz

Abstract

Superconducting hybrid structures can be described in a quasi-classical approximation, since all relevant states lie in close proximity to the Fermi surface. In the case of superconducting alloys, where a short mean free path of the particles is caused by a large impurity concentration, the system is described by isotropic Green's functions obeying the Usadel equation [1]. However, this equation must be completed by a set of boundary conditions. The goal of this work is to apply the quasi-classical theory of superconductivity to a diffusive Josephson junction consisting of a ferromagnet sandwiched between two superconductors. Boundary conditions will be calculated via a scattering matrix approach and be implemented numerically. The dependence of the critical current density on various parameters such as the *spin mixing angle* and temperature will be discussed.

Zusammenfassung

Heterogene supraleitende Strukturen können mittels einer quasiklassischen Näherung beschrieben werden, da alle relevanten Zustände des Systems in der Nähe der Fermi Energie liegen. Für supraleitende Legierungen, in denen eine kurze freie Weglänge durch eine hohe Verunreinigungskonzentration verursacht wird, können Systeme mit isotropen Green's Funktionen beschrieben werden, welche die Usadel Gleichung [1] erfüllen. Diese Gleichung muss allerdings durch Randbedingungen ergänzt werden. Das Ziel dieser Arbeit ist es, die quasiklassische Theory der Supraleitung auf diffusive Josephson Kontakte, bestehend aus einem Ferromagneten zwischen zwei Supraleitern, anzuwenden. Die Randbedingungen werden über einen Streumatrix-Ansatz berechnet sowie numerisch implementiert. Die Abhängigkeit der kritischen Stromdichte von verschiedenen Parametern, wie etwa dem *spin mixing angle* und der Temperatur, wird untersucht.

Contents

Introduction

Over 100 years ago, in 1911, the phenomenon of superconductivity was discovered by Kammerlingh-Onnes [2] in Leiden. After phenomenological descriptions by London and London [3] as well as Ginzburg and Landau [4] the first microscopic theory was developed by Bardeen, Cooper and Schrieffer in 1957 [5]. The success of the BCS-theory, honored with the Nobel price in 1972, is undeniable, as low temperature superconductors described by it are still subject to modern research. With further development of the theoretical tools by Gor'kov [6] in 1958, Green's functions replaced the pair wave function used in the original BCS-theory. The microscopic description, however, has practical drawbacks as much of the information contained in the Green's functions is not of interest for many effects. An easier formulation is given by the quasi-classical description developed by Eilenberger [7] and Larkin and Ovchinnikov [8]. These theories lay the foundation for a vast field of research involving superconducting systems. Since many years hybrid structures consisting for example of layered superconductor/ferromagnet systems are of particular interest. The close proximity and very different properties of these materials give rise to many physical phenomena such as the well known proximity effect [9], Andreev reflection [10, 11] and Josephson effect [12] as well as singlet-triplet mixing [13] and odd frequency pairing [14] as properties of each material can penetrate into the other. They find application for example in the field of spintronics [15] or the research of topological insulators [16]. The quasi-classical theory assumes that all relevant states lie in the vicinity of the Fermi surface of the superconductor, which results in an averaging over the momentum of the particles. This eliminates microscopic details and rapid spatial fluctuations of the Green's functions used. It makes the Green's functions itself easier to work with when attempting for example numerical calculations. The focus instead lies on the formulation of appropriate physical boundary conditions as the quasi-classical Green's function can show jumps at interfaces between the layers of the system. These jumps need to be calculated without the knowledge of the Green's function on the microscopic scale. For ferromagnetic interfaces that are the focus of this thesis, the boundary conditions were first derived by Zaitsev [17] for spin-active interfaces in the ballistic case in 1984. In the following years many generalizations to the original derivation have been developed [18, 19, 20, 21]. For the case of dirty superconductors, where strong elastic impurity scattering occurs due to high impurity densities, the Eilenberger transport equation [7] reduces to the Usadel equation [1]. This seemingly simpler description does not get reflected in the development of boundary conditions for spin-active interfaces that have only been derived in recent years [22, 23].

In this thesis the scattering matrix approach developed in [23] is outlined and applied to a superconductor/ferromagnet/superconductor hybrid structure in the dirty limit. The boundary conditions are used to calculate the density of the Josephson current [12] in dependence on various parameters.

Chapter 1

Theory

First, the Keldysh formalism for Green's functions that can be used for the description of superconducting systems will be introduced. From that, the main ideas of the quasi-classical theory of superconductivity developed by Eilenberger [7] and Larkin and Ovchinnikov [8] with the resulting transport equation for the quasi-classical Green's functions will be discussed. A more detailed look will be taken at the special case for dirty superconductors, the diffusive limit. Here, the Eilenberger transport equation reduces to the Usadel equation [1]. Lastly, boundary conditions for superconducting hybrid structures in the diffusive limit will be derived, following the work of Ref. [23].

1.1 Keldysh Green's functions

The tools provided by quantum mechanics are not cut out to describe complex systems containing up to the order of 10^{23} particles. Condensed matter physics studies systems like this so the more sophisticated framework of quantum field theory is used, which can be elegantly formulated using Green's functions. These functions are generalizations of expectation values of the field operators Ψ and $\Psi^\dagger$. One particular set are the Keldysh Green's functions [24], which are a central mathematical tool in modern superconductivity research.

The Keldysh Green's function have a 2×2 matrix structure in the so called Keldysh space, denoted with a "check" accent [25]

$$\check{\mathcal{G}} = \begin{pmatrix} \hat{\mathcal{G}}^{11} & \hat{\mathcal{G}}^{12} \\ \hat{\mathcal{G}}^{21} & \hat{\mathcal{G}}^{22} \end{pmatrix} \tag{1.1}$$

with the elements

$$\begin{aligned} \hat{\mathcal{G}}^{11}(1,1') &= -i\langle \mathcal{T}\left(\Psi(1)\Psi^\dagger(1')\right)\rangle \\ \hat{\mathcal{G}}^{12}(1,1') &= i\langle \Psi^\dagger(1')\Psi(1)\rangle \\ \hat{\mathcal{G}}^{21}(1,1') &= -i\langle \Psi(1)\Psi^\dagger(1')\rangle \\ \hat{\mathcal{G}}^{22}(1,1') &= -i\langle \tilde{\mathcal{T}}\left(\Psi(1)\Psi^\dagger(1')\right)\rangle\,. \end{aligned} \tag{1.2}$$

Here, the usual abbreviation $1 = (t_1, \mathbf{r}_1)$ for time and the spatial coordinates is used. The times t_1 and $t_{1'}$ of the component $\hat{\mathcal{G}}^{ij}(1,1')$ lie on the path c_i and c_j of the Keldysh contour in the complex plane, as shown in Fig. 1.1. $\mathcal{T}$ is the usual time ordering operator while $\tilde{\mathcal{T}}$ is the anti-time ordering operator, which gives the time ordering along the path c_2 in the lower half of the complex plane. The components of $\check{\mathcal{G}}$ are not linearly independent of one another and thus contain

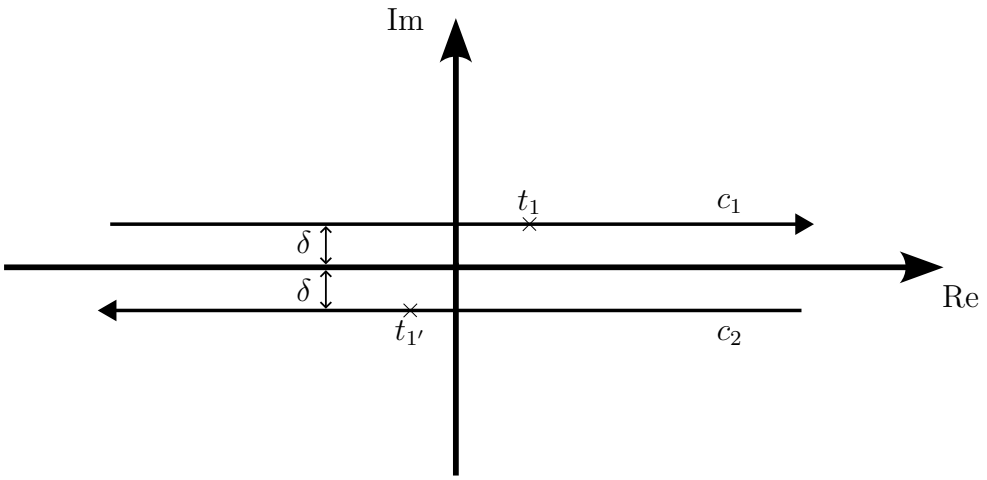

Fig. 1.1 The Keldysh contour with the paths c_1 and c_2 in the upper and lower half of the complex plane. They lie an infinitesimal distance δ away from the real axis. The imaginary times t_1 and $t_{1'}$ can lie on either path depending on the component of $\check{\mathcal{G}}$. Here, a possible configuration for $\hat{\mathcal{G}}^{12}$ is shown. Modified from [25].

redundant information. To eliminate these redundancies a linear transformation using the matrix $Q = (\hat{1} + \tau^3)/\sqrt{2}$ can be performed. The matrices $(\check{1}, \check{\tau}^1, \check{\tau}^2, \check{\tau}^3)$ are the Pauli matrices in Keldysh space. If the transformation $\check{\mathcal{G}} \to Q\hat{\mathcal{G}}Q^\dagger$ is performed, with matrix multiplication implied, one gets

$$\check{\mathcal{G}} = \begin{pmatrix} \hat{\mathcal{G}}^R & \hat{\mathcal{G}}^K \\ 0 & \hat{\mathcal{G}}^A \end{pmatrix} \tag{1.3}$$

for the full Green's function with the retarded, advanced and Keldysh component. The retarded and advanced parts of $\check{\mathcal{G}}$ are analytical in the upper and lower half of the complex plane respectively. The Keldysh Green's function obeys the Dyson equation of the form [26]

$$\check{\mathcal{G}} = \check{\mathcal{G}}^0 + \check{\mathcal{G}}^0 \otimes \check{\Sigma} \otimes \check{\mathcal{G}}\,, \tag{1.4}$$

where $\check{\mathcal{G}}^0$ is the Green's function for an ideal gas. The operation $A \otimes B$ for matrices A and B integrates over free spatial as well as time coordinates combined with a matrix multiplication [25]

$$(A \otimes B)(1, 1') = \int d^3\mathbf{x}_2 \int_{-\infty}^{\infty} dt_2 A(1,2)B(2,1')\,. \tag{1.5}$$

$\check{\Sigma}$ denotes the so called "self energy". In a diagrammatic formulation [24] the self energy is defined by all connected diagrams with one incoming and one outgoing line and is connected to $\check{\mathcal{G}}$ by the Dyson equation (1.4). It includes the superconducting order parameter Δ, information about impurity scattering and external potentials as well as molecular fields [23]. The structure of the self energy is similar to the structure of $\check{\mathcal{G}}$ in Eq. (1.3) with

$$\check{\Sigma} = \begin{pmatrix} \hat{\Sigma}^R & \hat{\Sigma}^K \\ 0 & \hat{\Sigma}^A \end{pmatrix} \tag{1.6}$$

containing the retarded, advanced and Keldysh self energies. These components, as elements of particle-hole space, which is denoted by the index of the matrices, are of the form [23]

$$\hat{\Sigma}^{R,A} = \begin{pmatrix} \Sigma^{R,A} & \Delta^{R,A} \\ \tilde{\Delta}^{R,A} & \tilde{\Sigma}^{R,A} \end{pmatrix}_{\mathrm{ph}}, \qquad \hat{\Sigma}^{K} = \begin{pmatrix} \Sigma^{K} & \Delta^{K} \\ -\tilde{\Delta}^{K} & -\tilde{\Sigma}^{K} \end{pmatrix}_{\mathrm{ph}} \tag{1.7}$$

with the tilde operation being defined as $\tilde{X}(\mathbf{p}_F, \mathbf{R}, E, t) = X(-\mathbf{p}_F, \mathbf{R}, -E, t)^*$.

For superconducting systems a spin dependence must be taken into account. This can be done by writing the spin-up and spin-down field operators as column matrices [26]

$$\hat{\Psi}_1 = \begin{pmatrix} \hat{\psi}_{1\uparrow} \\ \hat{\psi}^\dagger_{1\downarrow} \end{pmatrix}, \tag{1.8}$$

where the argument is written as an index for brevity. The product of two of these operators, as found in the definition of the Green's functions (1.2), is defined as the tensor product

$$\hat{\Psi}_1 \hat{\Psi}^\dagger_2 = \begin{pmatrix} \hat{\psi}_{1\uparrow}\hat{\psi}^\dagger_{2\uparrow} & \hat{\psi}_{1\uparrow}\hat{\psi}_{2\downarrow} \\ \hat{\psi}^\dagger_{1\downarrow}\hat{\psi}^\dagger_{2\uparrow} & \hat{\psi}^\dagger_{1\downarrow}\hat{\psi}_{2\downarrow} \end{pmatrix}. \tag{1.9}$$

The components of the superconducting Keldysh Green's functions are therefore elements in 2×2 spin space, otherwise the overall structure of the definitions and equations above stays the same.

1.2 Quasi-classical theory of superconductivity

A microscopic theory of superconductivity was first developed by Bardeen, Cooper and Schrieffer in 1957 [5]. This theory is based on an energetically favorable interaction between electrons and phonons resulting in an attraction between the electrons and consequently in the forming of so called Cooper pairs. These pairs of electrons have opposite spin and approximately opposite momenta. Therefore the total spin of the paired electrons is an integer and the Cooper pairs can condense into a superfluous state, very similar to the phenomenon of Bose-Einstein-condensation. This theory was developed further by Gor'kov, who formulated the microscopic description of superconductors in terms of Green's functions of the form (1.2) [6, 27, 28] in 1958. These Green's functions combined with a self-consistency equation for the superconducting order parameter Δ do contain all information of the system. However, this comes with the drawback of being hard to work with when implementing for numerical calculations. In many cases much of the information is not of particular interest, which led to the development of the quasi-classical approach by Eilenberger [7] and Larkin and Ovchinnikov [8] in 1968. The main idea is to integrate the Green's functions over the energy variable to average over microscopic fluctuations on atomic length scales.

The Green's function $\check{\mathcal{G}} = \check{\mathcal{G}}(t_1, \mathbf{r}_1, t_2, \mathbf{r}_2) \equiv \hat{\mathcal{G}}_{12}$ depends on the spatial coordinates $\mathbf{r}_1$ and $\mathbf{r}_2$ as well as the times t_1 and t_2. It changes on length scales given by the Fermi wavelength $\lambda_F = 2\pi/k_F$, which is often much smaller than the length

scales the physical effects of interest take place on. One can make a transition to new coordinates $\mathbf{R}$, T, $\mathbf{r}$, t defined by [26]

$$\begin{aligned} \mathbf{r}_1 &= \mathbf{R} - \frac{\mathbf{r}}{2} & \mathbf{r}_2 &= \mathbf{R} + \frac{\mathbf{r}}{2} \\ t_1 &= T - \frac{t}{2} & t_2 &= T + \frac{t}{2}\,, \end{aligned} \tag{1.10}$$

where $\mathbf{R}$ and T describe the motion of the center of mass, while $\mathbf{r}$ and t are the difference coordinates. These difference coordinates can be replaced in favor of the momentum $\mathbf{p}$ and energy E via the Fourier transformation

$$\check{\mathcal{G}}(\mathbf{R}, T, \mathbf{r}, t) = \int e^{-iEt} e^{i\mathbf{p}\cdot\mathbf{r}}\, \check{\mathcal{G}}(\mathbf{R}, T, \mathbf{p}, E)\, d\mathbf{p}\, dE \tag{1.11}$$

to get the so called Wigner or mixed representation of $\check{\mathcal{G}}$. With this representation the quasi-classical Green's function is defined by [26]

$$\check{g}(\mathbf{R}, T, \hat{p}, E) = \frac{i}{\pi} \int_{-\infty}^{\infty} d\varepsilon_{\mathbf{p}} \check{\mathcal{G}}(\mathbf{R}, T, \mathbf{p}, E) \tag{1.12}$$

with, for an assumed quadratic dispersion, $\varepsilon_{\mathbf{p}} = p^2/2m - \mu$ being the energy measured from the chemical potential μ, p the magnitude of the particle momentum and $\hat{p} = \mathbf{p}/p$ the unit vector in the momentum direction. Actually performing the integral in Eq. (1.12) is not as trivial as it might seem since the integrand does not fall off fast enough for the integral to converge. This problem can be solved via either introducing a cut-off energy or using contour integration [7]. The quasi-classical propagator $\check{g}$ does not depend on the magnitude of the particle momentum but just on its direction. The integration over the energy variable can be thought of as replacing the microscopic Green's function and their corresponding self energies by their value on the Fermi surface and then shifting information about the particle energy to a δ-function [26]

$$\check{\mathcal{G}}(\mathbf{R}, \mathbf{p}, t_1, t_2) \to \delta(\varepsilon_{\mathbf{p}}) \check{g}(\mathbf{R}, \hat{p}, t_1, t_2)\,. \tag{1.13}$$

With this approximation the quasi-particles described by $\check{g}$ move along trajectories varying on macroscopic length scales and can therefore be described classically, while still having the spin as well as particle-hole degrees of freedom treated quantum mechanically. The applicability of this approximation can be examined with the spectral function

$$A = \frac{i}{2\pi} \left(\hat{\mathcal{G}}^R - \hat{\mathcal{G}}^A \right) = -\frac{1}{\pi} \mathrm{Im} \left(\hat{\mathcal{G}}^R \right) \tag{1.14}$$

which, in equilibrium, is of the form of a sum of δ-functions at the energy of each state and therefore contains information about the spectrum of energy levels. In the quasi-classical approximation these δ-functions become, however, broadened, with the width defining the lifetime of each state. For the quasi-classical approximation to be justified the lifetime of the states must still be small compared to their energy [26].

The quasi-classical propagator $\check{g}$ defined in Eq. (1.12) is subject to the aforementioned Eilenberger-Larkin-Ovchinnikov transport equation and normalization condition [7, 8]

$$\left[E\check{\tau}^3 - \check{\Sigma}, \check{g}\right] + i\mathbf{v}_F \cdot \nabla_{\mathbf{R}}\check{g} = \check{0}\,, \qquad \check{g}\cdot\check{g} = \check{1}\,. \tag{1.15}$$

Here, $\mathbf{v}_F = \mathbf{v}_F(\mathbf{p}_F)$ is the Fermi velocity. The operator $\nabla_{\mathbf{R}}$ is the derivative with respect to the spatial coordinate R and $[A, B]$ denotes the commutator of matrices A and B.

1.3 The diffusive limit

Although Eq. (1.15) provides a much simpler description to complex superconducting systems than the microscopic one by the Gor'kov equations, there are still simplifications one could make. For practical applications the case of dirty superconductors of the BCS-type is of particular interest. For dirty superconductors, so called superconducting alloys, the (quasi-)particles get scattered with the impurity scattering rate $1/\tau_{\text{imp}}$, which is much larger than the relevant energies $k_B T_c$, E and $|\Delta|$ of the system. This leads to a diffusive motion rather than a ballistic one found in clean superconductors with low impurity densities. After having traveled a sufficiently long distance $x \gg l$, with l being the mean free path length, the impurity scattering leads to an isotropization of the particles motion. In this case the properties of the system do not depend on the momentum direction $\hat{p}$, but instead the average over all $\hat{p}$ is taken. For the quasi-classical Green's function $\check{g}$ one can do an expansion in spherical harmonics to first order in the momentum direction [26]

$$\check{g} \approx \check{G}_s + \hat{p}\check{g}_p\,. \tag{1.16}$$

with $\check{G}_s$ and $\check{g}_p$ being the s- and p-wave components of $\check{g}$, with $\check{g}_p \ll \check{G}_s$. Both components are independent of momentum direction. An analogous expansion can be done for the self energy

$$\check{\Sigma} \approx \check{\Sigma}_s + \hat{p}\check{\sigma}_p\,. \tag{1.17}$$

The Fermi momentum $\mathbf{v}_F = v_f\hat{p}$ can also be written explicitly with its magnitude v_f and its direction $\hat{p}$. Plugging this as well as Eqs. (1.16) and (1.17) into the Eilenberger equation (1.15) and omitting the index $\mathbf{R}$ for brevity leads to

$$\begin{aligned}\left[E\check{\tau}^3 - \check{\Sigma}_s, \check{G}_s\right] - \hat{p}\left[\check{\sigma}_p, \check{G}_s\right] + \hat{p}\left[E\check{\tau}^3 - \check{\Sigma}_s, \check{g}_p\right] - \hat{p}\cdot\hat{p}\left[\check{\sigma}_p, \check{g}_p\right] \\ + iv_F\hat{p}\cdot\nabla\check{G}_s + iv_F\hat{p}\cdot\hat{p}\cdot\nabla\check{g}_p = \check{0}\,.\end{aligned} \tag{1.18}$$

The term $\hat{p}\cdot\hat{p}\left[\check{\sigma}_p, \check{g}_p\right]$ is of second order in the p-wave components and can therefore be neglected. Splitting up the above equation in terms even and odd in $\hat{p}$ the expression

$$\left[E\check{\tau}^3 - \check{\Sigma}_s, \check{G}_s\right] + iv_F\hat{p}\cdot\hat{p}\cdot\nabla\check{g}_p = \check{0} \tag{1.19}$$

for the even contributions is obtained. Averaging over the momentum direction then results in

$$\left[E\check{\tau}^3 - \check{\Sigma}_s, \check{G}_s\right] + i\frac{1}{3}v_F\cdot\nabla\check{g}_p = \check{0}\,. \tag{1.20}$$

The odd contributions can be rewritten as

$$\left[E\check{\tau}^3 - \check{\Sigma}_s, \check{g}_p\right] - \left[\check{\sigma}_p, \check{G}_s\right] + iv_F \cdot \nabla \check{G}_s = \check{0}\,. \tag{1.21}$$

For strong elastic scattering the contribution of the commutator $\left[E\check{\tau}^3 - \check{\Sigma}_s, \check{g}_p\right]$ is small in comparison to the other terms and it can be neglected. For the other commutator one can rewrite it in terms of $\check{g}_p$ by using $\check{\sigma}_p = -i\check{g}_p/2\tau_{\mathrm{tr}}$, where τ_{tr} is the transport time in the theory of metals [26]. Using the normalization condition $\check{g} \cdot \check{g} = \check{1}$ from (1.15) together with Eq. (1.16) and neglecting terms of second order in $\check{g}_p$ leads to

$$\check{G}_s\,\check{G}_s + \hat{p}\check{G}_s\,\check{g}_p + \hat{p}\check{g}_p\,\check{G}_s = \check{1} \tag{1.22}$$

$$\Rightarrow \quad \check{G}_s\,\check{G}_s = \check{1}, \qquad \check{G}_s\,\check{g}_p + \check{g}_p\,\check{G}_s = \check{0}\,. \tag{1.23}$$

Therefore, the odd contribution (1.21) to the Eilenberger equation can be written as

$$iv_F \cdot \nabla \check{G}_s = \frac{i}{\tau_{\mathrm{tr}}} \check{G}_s\,\check{g}_p\,. \tag{1.24}$$

Multiplying both sides with $\check{G}_s$ and using its normalization from (1.23) an expression for the p-wave component of the quasi-classical propagator of

$$\check{g}_p = \tau_{\mathrm{tr}} v_F \check{G}_s \nabla \check{G}_s \tag{1.25}$$

can be obtained. Plugging this into Eq. (1.20) and realizing that $v_f \tau_{\mathrm{tr}}/3 = D$ is an expression for the diffusion coefficient finally results in

$$\left[E\check{\tau}^3 - \check{\Sigma}_s, \check{G}_s\right] + iD\nabla\left(\check{G}_s \nabla \check{G}_s\right) = \check{0}\,. \tag{1.26}$$

This is the Usadel equation [1], the transport equation for the isotropic part of the quasi-classical propagator $\check{G}_s$ in the limit of strong elastic scattering inside a dirty superconductor. One can further impose a normalization condition on $\check{G}_s$. In the scope of this thesis a pseudo-unitary normalization analogous to the one found in (1.15) of

$$\check{G}_s \cdot \check{G}_s = \check{1} \tag{1.27}$$

is chosen. With the knowledge of $\check{G}_s$ physical quantities such as the density of states or the current density can be calculated. For the latter the equation for the component $i \in \{x, y, z\}$ reads [23]

$$j_i = -e \sum_k \int_{-\infty}^{\infty} \frac{dE}{8} \operatorname{Tr}\left(N_F D_{ik} \hat{\tau}^3 \left[\check{G}_s \cdot \nabla \check{G}_s\right]^K\right) \tag{1.28}$$

with the diffusion tensor D, the elementary charge e and the density of states at the Fermi surface N_F. The arguments have again been omitted for brevity.

The components of $\check{G}_s$ further satisfy the symmetries

$$\begin{aligned} \hat{G}_s^A &= \left(\hat{\tau}^3 \hat{G}_s^R \hat{\tau}^3\right)^\dagger \\ \hat{G}_s^K &= -\left(\hat{\tau}^3 \hat{G}_s^K \hat{\tau}^3\right)^\dagger \\ \hat{G}_s^K &= \left(\hat{G}_s^R - \hat{G}_s^A\right) \tanh\left(\frac{E}{2k_B T}\right) \end{aligned} \tag{1.29}$$

on the real energy axis with the temperature T and the Boltzmann constant k_B. Here, a dependence of the Green's functions on temperature is introduced. For a BCS-superconductor the temperature influences the energy gap characterized by the magnitude of the order parameter $|\Delta| = |\Delta(T)|$. For the whole temperature range $0 \leq T \leq T_c$ the gap can be interpolated by [29, 30]

$$\Delta(T) = \Delta_0 \tanh\left(1.74\sqrt{\frac{T_c - T}{T}}\right) \tag{1.30}$$

with $\Delta_0 = \Delta(0) = 1.764 k_B T_c$. Here, T_c is the critical temperature of the superconductor.

Equations (1.15) or (1.26) provide a general starting point for numerical computation, but they must be completed by appropriate boundary conditions. Since in the quasi-classical approach fluctuations of the Green's function on atomic length scales are eliminated one is left with just the envelope of the microscopic fluctuations. And albeit being continuous on the microscopic scale the quasi-classical Green's function can contain jumps at boundaries and interfaces. To calculate these jumps without the information on the microscopic scale sophisticated methods such as transfer- [18], or in the case of this thesis, scattering matrix approaches [13, 23] are needed.

1.4 Boundary conditions

As outlined above the difficulty in the quasi-classical approach lies in the formulation of appropriate boundary conditions. These conditions are highly non-trivial and dedicated papers such as [17] exist for various systems for their derivation. Here, the work of Ref. [23] will be followed closely and a scattering matrix approach for the diffusive limit is employed in order to connect the quasi-classical propagators $\hat{g}$ and $\underline{\hat{g}}$ on the left and right side of a scattering interface with isotropic Green's functions $\hat{G}$ and $\underline{\hat{G}}$ away from the barrier, as shown in Fig. 1.2. In the following only the retarded part of the Green's functions will be considered as the other components can be calculated with the symmetries (1.29). The superscript R of the retarded Green's functions as well as the index s to emphasize $\hat{G}_s^R$ being isotropic are omitted for brevity.

To formulate the boundary conditions for a layered structure containing a half metal (S/H/S) or ferromagnet (S/F/S) scattering barrier in between to superconductors, first the normal state system (N/H/N or N/F/N) is considered. The scattering matrix connecting the amplitudes of incoming and outgoing waves on either side of the interface has the form of

$$\mathbf{S} = \begin{pmatrix} R & \underline{T} \\ T & \underline{R} \end{pmatrix}_{\leftrightarrows}, \tag{1.31}$$

with R and $\underline{R}$ being the reflection coefficients on the left and right side of the interface respectively, while T and $\underline{T}$ correspond to the transmission coefficients from left to right and right to left of the interface. The index $\leftrightarrows$ emphasizes that the components correspond to the reflection and transmission amplitudes. With this the connection

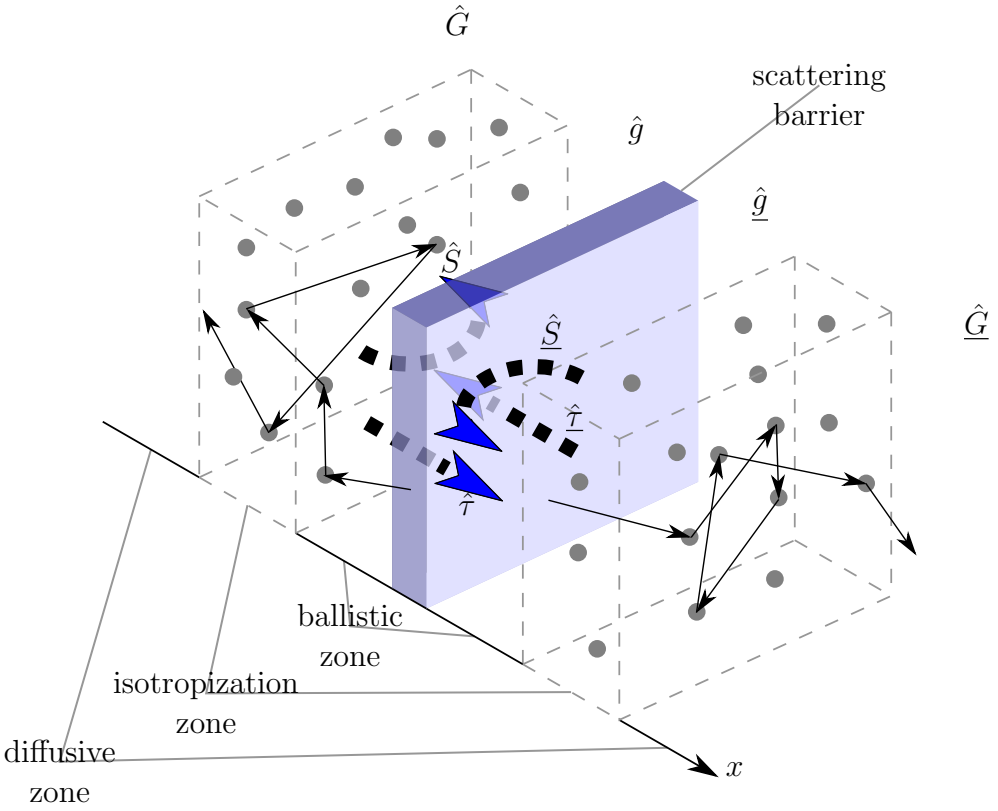

Fig. 1.2 Illustration of a layered superconducting system and the notation used. The quasi-classical propagators $\hat{g}$ and $\underline{\hat{g}}$ are ballistic Green's functions in close proximity to the scattering barrier. Particles moving away from the barrier scatter with impurities, which causes their motion to become isotropic. Deep inside the bulk of the superconductor the diffusive motion of the particles is described by the Usadel Green's functions $\hat{G}$ and $\underline{\hat{G}}$ respectively. Particles moving towards the scattering barrier can either get reflected or transmitted. The first case is described be the matrices $\hat{S}$ and $\underline{\hat{S}}$ for the left and right side of the interface respectively. The transmission is described by the hopping amplitudes $\hat{\tau}$ and $\underline{\hat{\tau}}$ for going from the left to right or right to left side of the barrier. Modified from [23].

between incoming and outgoing waves (index i and o respectively) is given by

$$\begin{pmatrix} \psi^o \\ \underline{\psi}^o \end{pmatrix} = \begin{pmatrix} R & \underline{T} \\ T & \underline{R} \end{pmatrix}_{\leftrightarrows} \cdot \begin{pmatrix} \psi^i \\ \underline{\psi}^i \end{pmatrix} . \tag{1.32}$$

For spin active interfaces such as ferromagnets, or multiple Fermi surfaces and thus scattering channels, the elements of $\mathbf{S}$ can further be matrices in spin and channel space. The wave functions ψ then have to be vectors appropriate to the structure of $\mathbf{S}$. For a general scattering matrix with dimensions $n \times n$ for R, $m \times m$ for $\underline{R}$, $n \times m$ for $\underline{T}$ and $m \times n$ for T one can decompose its components into a hermitian and an unitary part by writing for example the matrix R as

$$\begin{aligned} R &= \left(RR^\dagger\right)^{\frac{1}{2}} \left(RR^\dagger\right)^{-\frac{1}{2}} R \\ &= PU \end{aligned} \tag{1.33}$$
$$\text{with} \quad P = \left(RR^\dagger\right)^{\frac{1}{2}} \quad \text{and} \quad U = \left(RR^\dagger\right)^{-\frac{1}{2}} R\,,$$

where P is hermitian and U is unitary (see Appendix A.1). Analogously, the other components can be written as

$$\underline{R} = \underline{P}\,\underline{U}\,, \qquad T = QV\,, \qquad \underline{T} = \underline{Q}\underline{V} \tag{1.34}$$

as products of hermitian and unitary matrices as well. Now, $\hat{\mathbf{S}}$ shall be of the form

$$\hat{\mathbf{S}} = \begin{pmatrix} \sqrt{\hat{1} - CC^\dagger} & C \\ C^\dagger & -\sqrt{\hat{1} - C^\dagger C} \end{pmatrix}_{\leftrightarrows} \begin{pmatrix} S & 0 \\ 0 & \underline{S} \end{pmatrix}_{\leftrightarrows} \tag{1.35}$$

with the first matrix being hermitian and unitary matrices S, $\underline{S}$. The symbol $\hat{1}$ denotes, depending on the context, the $n \times n$ or $m \times m$ identity matrix. By carrying out the matrix multiplication the reflection and transmission matrices evaluate to

$$\begin{aligned} R &= \sqrt{\hat{1} - CC^\dagger}S & \underline{T} &= C\underline{S} \\ T &= C^\dagger S & \underline{R} &= -\sqrt{\hat{1} - C^\dagger C}\,\underline{S} \end{aligned} \tag{1.36}$$

Since $\sqrt{\hat{1} - CC^\dagger}$ and $\sqrt{\hat{1} - C^\dagger C}$ are hermitian, S and $\underline{S}$ are the unitary parts of the reflection matrices. Therefore, they can be identified with

$$S = U = \left(RR^\dagger\right)^{-\frac{1}{2}} R \tag{1.37}$$

$$-\underline{S} = \underline{U} = \left(\underline{R}\,\underline{R}^\dagger\right)^{-\frac{1}{2}} \underline{R}\,. \tag{1.38}$$

This then leads to an expression for C, which reads

$$C = -\underline{T}\,\underline{R}^\dagger \left(\underline{R}\,\underline{R}^\dagger\right)^{-\frac{1}{2}} \tag{1.39}$$

$$C^\dagger = -\left(\underline{R}\,\underline{R}^\dagger\right)^{-\frac{1}{2}} \underline{R}\,\underline{T}^\dagger\,. \tag{1.40}$$

The matrix C can also be expressed in different ways in terms of R and T, since the reflection and transmission matrices are not independent of one another because of particle conservation. This can be seen for example by calculating the "absolute value" squared of the transmission matrix $\underline{T}$, which leads to

$$\underline{T}\,\underline{T}^\dagger = C\underline{S}\,\underline{S}^\dagger C^\dagger = CC^\dagger\,, \tag{1.41}$$

since $\underline{S}$ is unitary. By plugging this result into the above expression for R in terms of C and S the resulting equation becomes

$$\begin{aligned} RR^\dagger &= \sqrt{\hat{1} - CC^\dagger}SS^\dagger \left[\sqrt{\hat{1} - CC^\dagger}\right]^\dagger \\ &= \hat{1} - CC^\dagger = \hat{1} - \underline{T}\,\underline{T}^\dagger \end{aligned} \tag{1.42}$$

so the usual expression to ensure particle conservation is obtained. The matrices S and $\underline{S}$ make up an auxiliary scattering matrix of an impenetrable interface

$$\mathbf{S}_0 = \begin{pmatrix} S & 0 \\ 0 & \underline{S} \end{pmatrix}_{\leftrightarrows}\,. \tag{1.43}$$

This matrix contains information about the phase shift of perfectly reflecting incoming waves. The transmission matrix C can further be parameterized with a matrix t as

$$C = \left(\hat{1} + tt^\dagger\right)^{-1} 2t\,, \tag{1.44}$$

with which the so called *hopping amplitudes*

$$\tau = t\underline{S} \qquad \underline{\tau} = t^\dagger S \tag{1.45}$$

are defined that describe the transmission of Bloch waves coming from the left or right side of the interface for τ and $\underline{\tau}$ respectively. This structure of the scattering matrix for the impenetrable interface encodes the reflection and transmission amplitudes. For further calculations the scattering matrix in particle hole space is needed. The auxiliary scattering matrices in particle hole space are obtained by using the "tilde"-symmetry [23], which, in the case of only one Fermi surface per superconductor and therefore a scalar structure in channel space, is given by [13]

$$\tilde{S}(k_\parallel) = S^{\mathrm{T}}(-k_\parallel)\,, \qquad \tilde{\tau}(k_\parallel) = S^{\mathrm{T}}(-k_\parallel)\tau^*(-k_\parallel)\underline{S}^{\mathrm{T}}(-k_\parallel) \tag{1.46}$$

and similarly for the underlined quantities. A^{T} denotes the transpose of the matrix A and $k_\parallel$ is the momentum component of a particle parallel to the interface, illustrated in Fig. 1.3.

The auxiliary scattering matrices and hopping amplitudes in particle hole space, now one for each side of the interface, are denoted by the "hat" accent and are of the form

$$\hat{S} = \begin{pmatrix} S & 0 \\ 0 & \tilde{S} \end{pmatrix} \qquad \hat{\tau} = \hat{\mathcal{S}}^\dagger \begin{pmatrix} \tau & 0 \\ 0 & \tilde{\tau} \end{pmatrix} \underline{\hat{\mathcal{S}}}^\dagger \tag{1.47}$$

and again analogous relations exist for the underlined quantities. Here, the matrices $\hat{\mathcal{S}}$ and $\underline{\hat{\mathcal{S}}}$ are defined by

$$\hat{\mathcal{S}} = \sqrt{\hat{S}} \qquad \underline{\hat{\mathcal{S}}} = \sqrt{\underline{\hat{S}}} \tag{1.48}$$

such that $\hat{\mathcal{S}}\hat{\mathcal{S}} = \hat{S}$ and $\underline{\hat{\mathcal{S}}}\,\underline{\hat{\mathcal{S}}} = \underline{\hat{S}}$. Since $\hat{S}$ is unitary, $\hat{\mathcal{S}}$ can also be chosen to be unitary. The multiplication of the hopping amplitude with the matrices $\hat{\mathcal{S}}^\dagger$ and $\underline{\hat{\mathcal{S}}}^\dagger$ make the relationship between the left and right side of the interface particulary easy as they remove spin mixing phases. With them one gets the simple relation $\hat{\tau} = \underline{\hat{\tau}}^\dagger$ between the hopping amplitudes on the left and right side of the interface. The scattering matrices in particle hole space as well as their square roots are unitary. In a similar manner the with respect to the Fermi velocity incoming and outgoing propagators in the ballistic zone (see Fig. 1.2) $\hat{g}_0^i$ and $\hat{g}_0^o$ for the auxiliary case of an impenetrable scattering barrier can be combined into a single propagator $\hat{g}_0$ via

$$\hat{g}_0^i = \hat{\mathcal{S}}^\dagger \hat{g}_0 \hat{\mathcal{S}} \qquad \hat{g}_0^o = \hat{\mathcal{S}}\hat{g}_0\hat{\mathcal{S}}^\dagger \tag{1.49}$$

and the propagator $\underline{\hat{g}}_0$ for the right side of the interface is defined analogously. With that the boundary conditions for the auxiliary case in the ballistic zone [23]

$$\hat{g}_0^o = \hat{S}\,\hat{g}_0^i\,\hat{S}^\dagger\,, \qquad \underline{\hat{g}}_0^o = \underline{\hat{S}}\,\underline{\hat{g}}_0^i\,\underline{\hat{S}}^\dagger \tag{1.50}$$

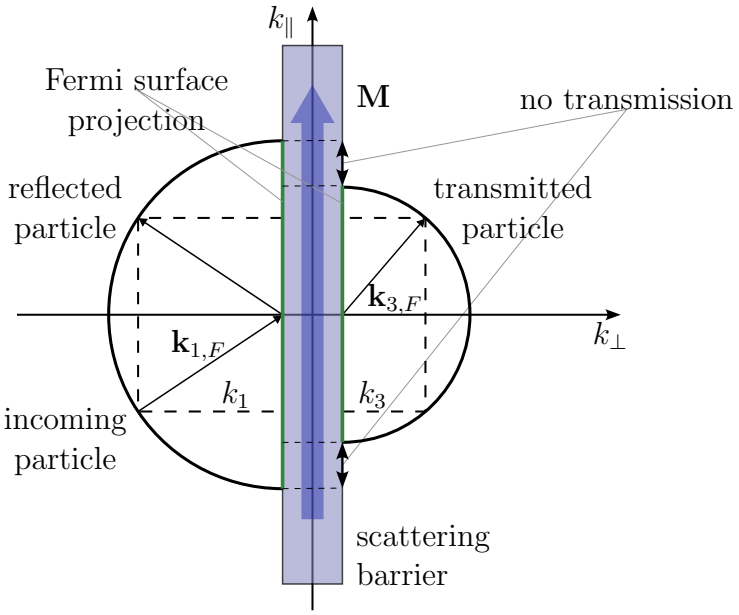

Fig. 1.3 Reflection and transmission in reciprocal space for a particle coming from the left of the scattering barrier with magnetization **M** parallel to the interface. The total momenta for spherical Fermi surfaces in left and right regions are $k_{F,1,3} = \sqrt{k_{1,3}^2 + k_\parallel^2}$ respectively. The momentum component parallel to the interface $k_\parallel$ is conserved in the scattering process. The projection of the Fermi surfaces are circles, shown schematically in green. There exists a region in between the smaller and larger Fermi surface, where no transmission can occur, since all allowed states lie on the Fermi surface.

become trivial. The connection of these ballistic propagators to the Green's functions $\hat{G}$ and $\underline{\hat{G}}$ at the beginning of the isotropization zone cannot be derived in the scope of the quasi-classical theory of superconductivity, but instead the microscopic description using Gor'kov Green's functions is used [31, 22]. With the matrices

$$\hat{G}_1 = \hat{\mathcal{S}}^\dagger \, \hat{G} \, \hat{\mathcal{S}} \qquad \hat{G}_2 = \hat{\mathcal{S}} \, \hat{G} \, \hat{\mathcal{S}}^\dagger \tag{1.51}$$

the dependence of the auxiliary ballistic propagator on the isotropic Green's function reads in four equivalent formulations [23]

$$\hat{g}_0 + \hat{1} = 2 \left(\hat{1} + \hat{G}_2 \hat{G}_1 \right)^{-1} \left(\hat{G}_2 + \hat{1} \right) \tag{1.52a}$$

$$= 2 \left(\hat{G}_1 + \hat{1} \right) \left(\hat{1} + \hat{G}_2 \hat{G}_1 \right)^{-1} \tag{1.52b}$$

$$\hat{g}_0 - \hat{1} = 2 \left(\hat{1} + \hat{G}_1 \hat{G}_2 \right)^{-1} \left(G_1 - \hat{1} \right) \tag{1.52c}$$

$$= 2 \left(\hat{G}_2 - \hat{1} \right) \left(\hat{1} + \hat{G}_1 \hat{G}_2 \right)^{-1} \tag{1.52d}$$

and again, these equation hold true for the underlined quantities as well. The equivalence is shown in Appendix A.2. Next, for the sake of simpler notation the propagator

$$\hat{g}_1 = \hat{\tau} \, \underline{\hat{g}}_0 \, \hat{\tau}^\dagger \tag{1.53}$$

will be introduced with which a t-matrix [23, 13, 32]

$$\hat{t} = \left(\hat{1} + \hat{g}_1 \hat{g}_0 \right)^{-1} \hat{g}_1 \tag{1.54}$$

can be formally calculated. With this, the full propagators for incoming and outgoing directions $\hat{g}^i$ and $\hat{g}^o$ can be calculated via

$$\hat{g}^i = \hat{g}_0 - \left(\hat{g}_0 - \hat{1}\right) \hat{t} \left(\hat{g}_0 + \hat{1}\right) \tag{1.55}$$

$$\hat{g}^o = \hat{g}_0 - \left(\hat{g}_0 + \hat{1}\right) \hat{t} \left(\hat{g}_0 - \hat{1}\right) \, . \tag{1.56}$$

These propagators are solutions to the ballistic problem for a scattering barrier with non-zero transmission. Lastly, one must relate them to the isotropic Green's functions by formulation of the desired boundary conditions for $\hat{G}$ and $\underline{\hat{G}}$. This can be done by introducing the so called *matrix current* $\hat{\mathcal{I}}$ [31, 22]. This quantity originates from circuit theory developed by Nazarov [33], where superconducting systems are treated similarly to electrical circuits. The matrix current holds information about the flow of charge as well as spin and electron-hole decoherence and is conserved in the isotropization zone [23]. The relation of the matrix current and the full propagators reads

$$\hat{\mathcal{I}} = \hat{\mathcal{S}} \hat{g}^o \hat{\mathcal{S}}^\dagger - \hat{\mathcal{S}}^\dagger \hat{g}^i \hat{\mathcal{S}} \, . \tag{1.57}$$

Finally, the boundary condition for the Green's function in the isotropization regions in the case of a two-dimensional spherical Fermi surfaces can be written as [23]

$$\mathcal{G}_q \int_0^{k_F} \frac{\hat{\mathcal{I}}}{2\pi} k_\parallel \, dk_\parallel = -\sigma \hat{G} \frac{d}{dx} \hat{G} \tag{1.58}$$

with the quantum of conductance $\mathcal{G}_q = e^2/h$, the conductivity per spin $\sigma = e^2 N_F D$, where the Planck constant h and the elementary charge e are written explicitly for clarity. N_F is the density of states at the Fermi surface and D is the diffusion constant. The magnitude of the Fermi wave vector k_F equals the radius of the larger of the two Fermi surfaces left and right of the interface, illustrated in Fig. 1.3. It can be calculated via

$$k_F = \sqrt{2 \left[E_F - \min(V_1, V_3) \right]} \, . \tag{1.59}$$

Chapter 2

Application

The scattering matrix approach discussed in Sec. 1.4 is applied to a superconductor/ferromagnet/superconductor-structure (S/F/S-structure). The scattering matrix and hopping amplitudes as well as the solution to the homogeneous Usadel-equation are calculated. These quantities go into the previously discussed boundary conditions and allow one to calculate the current density in dependence of various parameters. The numerical implementation will be discussed briefly.

2.1 Interface scattering matrix

The system of interest consists of two dirty superconductors separated by a ferromagnetic barrier. The magnetization of the ferromagnet shall be in the z-direction, parallel to the interfaces with the superconductors as shown in Fig. 1.3. The interface is assumed to be atomically smooth and planar. The magnetization introduces two different scattering potentials for incoming electrons, depending on their spin. To formulate the boundary conditions for this system, a scattering matrix approach [23] is employed, where first the interface scattering matrix for an impenetrable interface in the normal state is calculated. In the next step, auxiliary propagators subject to these impenetrable boundary conditions are calculated with the help of the homogeneous solutions to the Usadel transport equation and normalization condition (1.26). Finally, this leads to a matrix current which again goes into the Usadel equation as a boundary condition.

First, the scattering matrix of a normal state system consisting of a spin independent potential barrier with height V_2 and different potentials V_1 and V_3 to the left and right will be calculated. The scattering matrix will be of the form (1.31)

$$\mathbf{S} = \begin{pmatrix} R & \underline{T} \\ T & \underline{R} \end{pmatrix}_{\leftrightarrows} . \tag{2.1}$$

Here, R and $\underline{R}$ are the reflection coefficients on the left and right side of the interface respectively. T and $\underline{T}$ are the transmission coefficient that characterizes a particle going from left to right of the barrier and vice versa. A schematic depiction of a particle scattering on the left side of the barrier can be seen in Fig. 2.1. To calculate R and T a constant particle current with Fermi energy E_F going from left to right is considered. For a smooth interface parallel to the y-z-plane, the momentum component parallel to the interface $\mathbf{k}_\parallel$ will be conserved and the problem reduces to a one dimensional one. The Hamilton operator for the region $j \in \{1, 2, 3\}$ is given by

$$\mathcal{H}_j = \left(-\frac{1}{2} \left(\frac{d^2}{dx^2} + \frac{d^2}{dy^2} + \frac{d^2}{dz^2} \right) + V_j \right) , \tag{2.2}$$

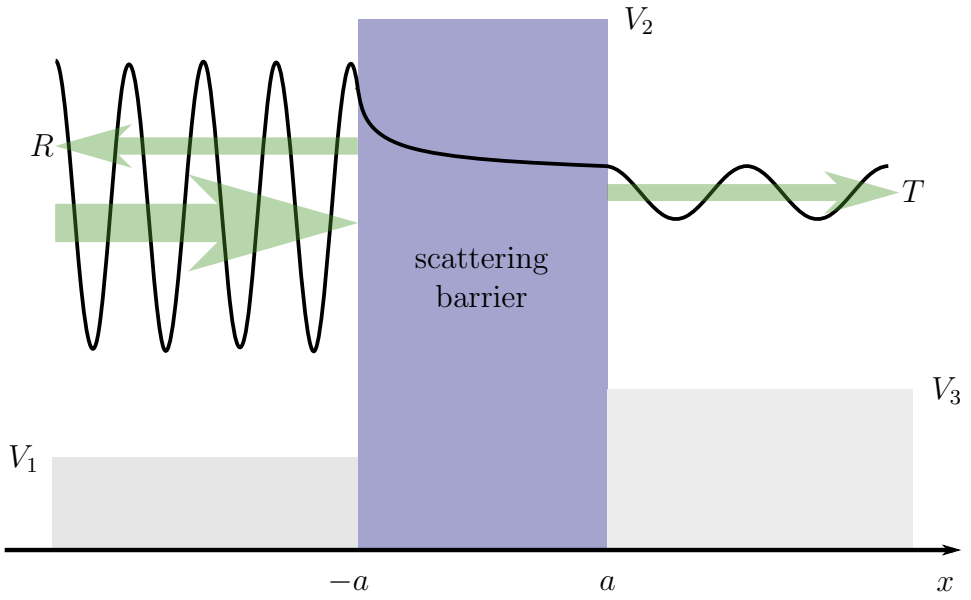

Fig. 2.1 Schematic depiction of the wave function of a particle coming from the left and scattering with a potential barrier of width $2a$ and height V_2. The left and right side of the interface have constant potential of V_1 and V_3 respectively. The amplitude of the reflected part is described by R, while the transmission is described be T. These quantities contain information about the reflection and transmission probabilities $P_R = |R|^2$ and $P_T = |T|^2$, with $P_R + P_T = 1$, as well as the phase shift caused by the scattering.

with $\hbar = m = 1$ for simplicity. In the case of a quadratic dispersion relation the Fermi energy in the regions (1) and (3) left and right to the scattering barrier can be expressed as

$$\begin{aligned} T_j + V_j &= E_F \\ \frac{1}{2}\left(\mathbf{k}_j^2 + \mathbf{k}_\parallel^2\right) + V_j &= E_F \end{aligned} \tag{2.3}$$

for $j \in \{1, 3\}$. All energies are measured from the chemical potential $\mu = 0$. Therefore, the corresponding momentum components are defined as

$$k_j = \sqrt{2(E_F - V_j) - k_\parallel^2} \tag{2.4}$$

with $k = |\mathbf{k}|$. For region (2) inside the potential barrier, the wave vector will be defined as

$$\kappa = \sqrt{2(V_2 - E_F) + k_\parallel^2}\,. \tag{2.5}$$

The incoming particle current can be describes as a plane wave, which leads to the usual ansatz for the wave function of the form

$$\psi_{E_F}(x) = \begin{cases} \dfrac{1}{\sqrt{k_1}}\left(e^{ik_1(x+a)} + Re^{-ik_1(x+a)}\right) & : \quad -\infty < x \leq -a \\ Ae^{\kappa x} + Be^{-\kappa x} & : \quad -a < x \leq a \\ \dfrac{1}{\sqrt{k_3}} Te^{ik_3(x-a)} & : \quad a < x < \infty \end{cases}. \tag{2.6}$$

The factor $1/\sqrt{k_j}$ ensures normalization of the particle current. The reflected and transmitted portions of the wave are described by $Re^{-ik_1(x+a)}$ and $Te^{ik_3(x-a)}$ respectively. One now needs to match the wave functions through imposing the conditions

$$\begin{aligned} \psi_{E_F}(-a_-) &= \psi_{E_F}(-a_+) \\ \frac{d}{dx}\psi_{E_F}\Big|_{x=-a_-} &= \frac{d}{dx}\psi_{E_F}\Big|_{x=-a_+} \\ \psi_{E_F}(a_-) &= \psi_{E_F}(a_+) \\ \frac{d}{dx}\psi_{E_F}\Big|_{x=a_-} &= \frac{d}{dx}\psi_{E_F}\Big|_{x=a_+} \end{aligned} \tag{2.7}$$

at the boundary of the scattering barrier to ensure continuity and differentiability of the wave function. The index of a indicates that a limit is taken from the right $(+)$ or the left $(-)$. Plugging in the wave function (2.6) one can solve for the reflection and transmission amplitudes R and T. By respectively adding the first and second as well as the third and fourth condition of (2.7) and plugging in (2.6) the equations

$$\frac{1}{\sqrt{k_1}}(1+R) + i\frac{\sqrt{k_1}}{\kappa}(1-R) = 2Ae^{-\kappa a} \tag{2.8}$$

$$\left(\frac{1}{\sqrt{k_3}} + i\frac{\sqrt{k_3}}{\kappa}\right) T = 2Ae^{\kappa a} \tag{2.9}$$

to eliminate the coefficient A, which is not of interest, are obtained. Similarly, to eliminate B one needs to subtract the pairs of equations instead of adding them. This leads to

$$\frac{1}{\sqrt{k_1}}(1+R) - i\frac{\sqrt{k_1}}{\kappa}(1-R) = 2Be^{\kappa a} \tag{2.10}$$

$$\left(\frac{1}{\sqrt{k_3}} - i\frac{\sqrt{k_3}}{\kappa}\right) T = 2Be^{-\kappa a}\,. \tag{2.11}$$

By rearranging the above equations to get two expressions for each coefficient A and B these can be set equal to get the two equations

$$\frac{1}{\sqrt{k_1}}(1+R) + i\frac{\sqrt{k_1}}{\kappa}(1-R) = e^{-2\kappa a}\left(\frac{1}{\sqrt{k_3}} + i\frac{\sqrt{k_3}}{\kappa}\right) T \tag{2.12}$$

$$\frac{1}{\sqrt{k_1}}(1+R) - i\frac{\sqrt{k_1}}{\kappa}(1-R) = e^{2\kappa a}\left(\frac{1}{\sqrt{k_3}} - i\frac{\sqrt{k_3}}{\kappa}\right) T\,. \tag{2.13}$$

The above expressions can further be simplified again by addition and subtraction of the equations. This leads to

$$\frac{1}{\sqrt{k_1}}(1+R) = \frac{1}{\sqrt{k_3}} T\cosh 2\kappa a - i\frac{\sqrt{k_3}}{\kappa} T\sinh 2\kappa a \tag{2.14}$$

$$i\frac{\sqrt{k_1}}{\kappa}(1-R) = i\frac{\sqrt{k_3}}{\kappa} T\cosh 2\kappa a - \frac{1}{\sqrt{k_3}} T\sinh 2\kappa a\,. \tag{2.15}$$

These expressions can be written in an easier way by introducing the real valued quantities

$$\begin{aligned} s &= \sinh 2\kappa a & c &= \cosh 2\kappa a \\ \alpha &= \sqrt{\frac{k_1}{k_3}} & \beta &= \frac{\sqrt{k_1 k_3}}{\kappa}\,. \end{aligned} \tag{2.16}$$

Employing the new notation and rewriting the above system of equations for the coefficients R and T in matrix form results in

$$\begin{pmatrix} -1 & \alpha c - i\beta s \\ 1 & \alpha^{-1}c - (i\beta)^{-1}s \end{pmatrix} \cdot \begin{pmatrix} R \\ T \end{pmatrix} = \begin{pmatrix} 1 \\ 1 \end{pmatrix} . \tag{2.17}$$

Now the solution for R and T can simply be obtained via matrix inversion and multiplication. After some algebra (see Appendix A.3) one arrives at the solution

$$\begin{pmatrix} R \\ T \end{pmatrix} = \frac{1}{(\alpha + \alpha^{-1})c - i(\beta - \beta^{-1})s} \begin{pmatrix} (\alpha - \alpha^{-1})c - i(\beta + \beta^{-1})s \\ 2 \end{pmatrix} . \tag{2.18}$$

Analogously, the amplitudes for an incoming wave from the right can be calculated by making the substitutions $k_{1,3} \to k_{3,1}$ and $x \to -x$ to get the coefficients $\underline{R}$ and $\underline{T}$. In the above notation, this translates to $\alpha \to \alpha^{-1}$, while the other variables stay the same, as can be easily seen from (2.16). With that the scattering matrix in the reflection and transmission components becomes

$$\hat{\mathbf{S}}(k_1, k_2, k_3, a) = \begin{pmatrix} R & \underline{T} \\ T & \underline{R} \end{pmatrix}_{\leftrightarrows} = \begin{pmatrix} \Gamma r & \Gamma \\ \Gamma & -\Gamma r^* \end{pmatrix}_{\leftrightarrows} \tag{2.19}$$

with

$$\Gamma = \frac{2}{(\alpha + \alpha^{-1})c - i(\beta - \beta^{-1})s} \tag{2.20}$$

$$r = \frac{(\alpha - \alpha^{-1})c - i(\beta + \beta^{-1})s}{2} . \tag{2.21}$$

For a ferromagnetic barrier the scattering potential is different depending on the spin of the incoming particle. To account for this the wave numbers

$$\kappa^{\uparrow,\downarrow} = \sqrt{2\left(V_2^{\uparrow,\downarrow} - E_F\right) + k_\parallel} \tag{2.22}$$

for spin up or spin down particles respectively are introduced. Similarly, each quantity with the superscript $\uparrow$ or $\downarrow$ will depend on $\kappa^\uparrow$ or $\kappa^\downarrow$ respectively instead of the κ used for the spin independent case. This leads to a normal state scattering matrix for the spin dependent system of

$$\begin{aligned} \hat{\mathbf{S}} &= \begin{pmatrix} R^\uparrow & 0 & \underline{T}^\uparrow & 0 \\ 0 & R^\downarrow & 0 & \underline{T}^\downarrow \\ T^\uparrow & 0 & \underline{R}^\uparrow & 0 \\ 0 & T^\downarrow & 0 & \underline{R}^\downarrow \end{pmatrix}_{\leftrightarrows} = \begin{pmatrix} \Gamma^\uparrow r^\uparrow & 0 & \Gamma^\uparrow & 0 \\ 0 & \Gamma^\downarrow r^\downarrow & 0 & \Gamma^\downarrow \\ \Gamma^\uparrow & 0 & -\Gamma^\uparrow r^{\uparrow *} & 0 \\ 0 & \Gamma^\downarrow & 0 & -\Gamma^\downarrow r^{\downarrow *} \end{pmatrix}_{\leftrightarrows} \\ &= \begin{pmatrix} \hat{\mathbf{S}}_{11} & \hat{\mathbf{S}}_{12} \\ \hat{\mathbf{S}}_{21} & \hat{\mathbf{S}}_{22} \end{pmatrix}_{\leftrightarrows} \end{aligned} \tag{2.23}$$

with the elements $\hat{\mathbf{S}}_{ij}$ being 2×2-matrices in spin space. Under the assumption of particle conservation the reflection- and transmission amplitudes must add up to unity. With the substitution introduced above this condition reads

$$\left|\Gamma^{\uparrow,\downarrow}\right|^2 \left(\left|r^{\uparrow,\downarrow}\right|^2 + 1\right) = 1 . \tag{2.24}$$

The scattering matrix, as shown in (1.35), can be written as

$$\hat{\mathbf{S}} = \begin{pmatrix} \sqrt{\hat{1} - CC^\dagger} & C \\ C^\dagger & -\sqrt{\hat{1} - C^\dagger C} \end{pmatrix}_{\leftrightarrows} \begin{pmatrix} S & 0 \\ 0 & \underline{S} \end{pmatrix}_{\leftrightarrows} , \tag{2.25}$$

where the matrices S and $\underline{S}$ are now unitary matrices in spin space. For this particular system they evaluate to

$$\begin{pmatrix} S & 0 \\ 0 & \underline{S} \end{pmatrix}_{\leftrightarrows} = \mathrm{diag} \left(\frac{\Gamma^\uparrow r^\uparrow}{|\Gamma^\uparrow r^\uparrow|}, \frac{\Gamma^\downarrow r^\downarrow}{|\Gamma^\downarrow r^\downarrow|}, \frac{\Gamma^\uparrow r^{\uparrow *}}{|\Gamma^\uparrow r^\uparrow|}, \frac{\Gamma^\downarrow r^{\downarrow *}}{|\Gamma^\downarrow r^\downarrow|} \right)_{\leftrightarrows} . \tag{2.26}$$

The transmission matrix C can be parametrized as in Eq. (1.44). The matrix t can be calculated by carrying out a singular value decomposition (SVD) on C.

$$C = u\delta v^\dagger = \begin{pmatrix} -\frac{r^\uparrow}{|r^\uparrow|} & 0 \\ 0 & -\frac{r^\downarrow}{|r^\downarrow|} \end{pmatrix} \begin{pmatrix} \left|\Gamma^\uparrow\right| & 0 \\ 0 & \left|\Gamma^\downarrow\right| \end{pmatrix} \hat{1} . \tag{2.27}$$

The SVD of t then reads

$$\begin{aligned} t &= u \left[\left(1 - \sqrt{1 - \delta^2} \right) \delta^{-1} \right] v^\dagger \\ &= \begin{pmatrix} -\frac{r^\uparrow}{|\Gamma^\uparrow r^\uparrow|} \left(1 - \left|\Gamma^\uparrow r^\uparrow\right| \right) & 0 \\ 0 & -\frac{r^\downarrow}{|\Gamma^\downarrow r^\downarrow|} \left(1 - \left|\Gamma^\downarrow r^\downarrow\right| \right) \end{pmatrix} , \end{aligned} \tag{2.28}$$

where the relation (2.24) between Γ and r was used. With the matrix t the hopping amplitude matrices are defined as in Eq. (1.45). Since $\hat{S}$ and $\underline{\hat{S}}$ are diagonal matrices not only in particle hole but also spin space, the matrix square root becomes trivial and will be calculated by taking the principal square root of each element individually in order to get $\hat{\mathcal{S}}$ and $\underline{\hat{\mathcal{S}}}$ according to Eq. (1.48).

2.2 Homogeneous solution of the Usadel equation

One may have noted that in order to formulate the boundary condition (1.58) and acquire the desired solution for the isotropic Green's function, this exact Green's function is already used in the process. This might raise the concern that Eq. (1.51) and everything which comes after that is of no use. However, even if one does not know the exact $\hat{G}$, an initial guess from which a new $\hat{G}$ can be calculated using the outlined procedure, can be made. This process could then be repeated with the newly calculated Green's function and sooner or later a solution with some desired numerical accuracy would be obtained. The initial guess of $\hat{G}$ in the scope of this thesis will be the solution of the homogeneous Usadel equation

$$\left[E\hat{\tau}^3 - \hat{\Delta}, \hat{G} \right] = \hat{0} . \tag{2.29}$$

This equation is the retarded part of Eq. (1.26) where $\hat{G}$ is taken to be independent on the spatial coordinates, such that $\nabla\hat{G} = \hat{0}$ and the second term vanishes. The self-energy $\check{\Sigma}_s^R$ is replaced with the order parameter matrix $\hat{\Delta} = \mathrm{adiag}\,(\Delta, -\Delta, \Delta^*, -\Delta^*)$

with $\hat{A} = \mathrm{adiag}\,(A_{1,n}, A_{2,n-1}, \dots)$ denoting an anti-diagonal $n \times n$-matrix $\hat{A}$ with components A_{ij}. Equation (2.29) shows that $\hat{G}$ and $E\hat{\tau}^3 - \hat{\Delta}$ commute. Therefore, the ansatz

$$\hat{G} = q\left(E\hat{\tau}^3 - \hat{\Delta}\right), \tag{2.30}$$

can be made, where q is determined through the normalization condition $\hat{G}\cdot\hat{G} = \hat{1}$ analogous to Eq. (1.27). The leads to the normalized homogeneous solution

$$\hat{G}_{\mathrm{hom}} = \pm\frac{1}{\sqrt{(E+i\delta)^2 - |\Delta|^2}}\left((E+i\delta)\hat{\tau}^3 - \hat{\Delta}\right). \tag{2.31}$$

Here the substitution $E \to E + i\delta$ is made, with δ being an infinitesimal positive real number, to ensure that $\hat{G}$ lies in the upper half of the complex plane, because it is a retarded Green's function. The expression for $\underline{\hat{G}}_{\mathrm{hom}}$ can be found analogously. In the following implementation the solution with the positive sign is taken for both the left and right side of the interface. The solutions to the homogeneous Usadel equation together with the auxiliary scattering matrices S and $\underline{S}$ as well as the matrix t, given by Eqs. (2.26) and (2.28) respectively, can now be used to explicitly calculate the boundary conditions for the isotropic Green's functions $\hat{G}$ as shown in Sec. 1.4. This marks the starting point of the numerical calculations for the matrix current $\hat{\mathcal{I}}$ used to calculate the current density of the system in dependence on various parameters, which will be discussed in chapter 3.

2.3 Current density of the S/F/S hybrid structure

In order to obtain the current density $\mathbf{j}$ of the system of interest to reasonable accuracy it is not necessary to solve the Usadel equation (1.26) with the boundary condition (1.58) iteratively. This is due to the fact that $\mathbf{j}$ contains the term $\left[\check{G}\cdot\nabla\check{G}\right]^K$, which is already very similar to the right hand side of Eq. (1.58). Doing the matrix multiplication explicitly, one gets for the needed Keldysh component

$$\left[\check{G}\cdot\nabla\check{G}\right]^K = \hat{G}^R\cdot\nabla\hat{G}^K + \hat{G}^K\cdot\nabla\hat{G}^A. \tag{2.32}$$

Using the relations (1.29) as well as the normalization condition $\hat{G}^R\cdot\hat{G}^R = \hat{1}$, the right hand side of Eq. (2.32) can be written only in terms of the retarded Green's function (see Appendix A.4) as

$$\left[\check{G}\cdot\nabla\check{G}\right]^K = \tanh\left(\frac{E}{2k_BT}\right)\left[\hat{G}^R\cdot\nabla\hat{G}^R + \hat{\tau}^3\left(\hat{G}^R\cdot\nabla\hat{G}^R\right)^\dagger\hat{\tau}^3\right]. \tag{2.33}$$

By introducing the diffusive coherence length at the critical temperature [34]

$$\xi_D = \sqrt{\frac{\hbar D}{2\pi k_B T_c}} \tag{2.34}$$

as a characteristic length scale, the substitution $\nabla \to \xi_D^{-1} d/d\xi$ with $\xi = x/\xi_D$ can be made. Plugging this as well as Eq. (2.33) into Eq. (1.28), omitting the superscript R for brevity and assuming a scalar diffusion constant, one gets

$$j_x = -\frac{eN_F D}{\xi_D} \int_{-\infty}^{\infty} \frac{dE}{8} \tanh\left(\frac{E}{2k_B T}\right) \mathrm{Tr}\left(\hat{\tau}^3 \hat{G} \frac{d}{d\xi} \hat{G} + \left(\hat{G} \frac{d}{d\xi} \hat{G}\right)^{\dagger} \hat{\tau}^3\right) \tag{2.35}$$

for the component of the current density in x-direction. In the integrand, the term $\tanh(E/2k_BT)$ takes the role of a distribution function related to the Fermi distribution function f_F via [26]

$$\tanh\left(\frac{E}{2k_B T}\right) = 1 - 2f_F(E)\,. \tag{2.36}$$

The above expression for the current density must, however, be rewritten in a more convenient way. Equation (2.35) is only correct for real energies E, as the term $\left(\hat{G}^R \cdot \nabla \hat{G}^R\right)^{\dagger}$is analytical in the lower half of the complex plane, while $\hat{G}^R \cdot \nabla \hat{G}^R$ is analytical in the upper half. This problem can be solved by noticing that inside the trace operation a matrix and its hermitian conjugate get added, which eliminates the imaginary part of each component. Therefore, Eq. (2.35) can be rewritten as

$$j_x = -\frac{eN_F D}{\xi_D} \mathrm{Re}\left[\int_{-\infty}^{\infty} \frac{dE}{4} \tanh\left(\frac{E + i\delta}{2k_B T}\right) \mathrm{Tr}\left(\hat{\tau}^3 \hat{G} \frac{d}{d\xi} \hat{G}\right)\right]\,, \tag{2.37}$$

where the distribution function is shifted into the upper half of the complex plane in order to be consistent with the substitution made in Eq. (2.31). The Green's functions $\hat{G}^R = \hat{G}^R(E + i\delta)$ now depends on the complex energy $E + i\delta$ lying in the upper half of the complex plane as well.

2.4 Numerical implementation

The scattering matrix approach for the most part is trivial to implement into numerical calculations. The equations (1.49) to (1.57) just contain multiplication and inversion of unit-less matrices. These operations have optimized routines commonly used and can therefore be executed fast and with very high precision. By introducing the length scale $k_0^{-1} = k_1^{-1}(k_\parallel = 0)$, the wave vectors as well as the width of the scattering barrier will be expressed in terms of k_0 or k_0^{-1} respectively, so for example, the expression for $c = \cosh 2\kappa a$ in (2.16) will be written as $c = \cosh(2(\kappa/k_0)(k_0 a))$. The two largest sources of numerical error as well as long run times are the integrals in Eq. (1.58) and (2.37). For the first a straight forward solution to cut down run time is to only integrate the relevant components. Combining the boundary condition (1.58) and (2.37) in the aforementioned way one may realize that due to the trace operation only the elements on the main diagonal of $\hat{\mathcal{I}}$ contribute to the current density. This reduces the number of components to integrate by a factor of four from 16 to 4, since $\hat{\mathcal{I}}$ is a 4×4 matrix in combined spin and particle-hole space.

The integral over the energy in Eq. (2.37) requires a more sophisticated treatment. The substitution $E \to E + i\delta$ introduced in Eq. (2.31) for the homogeneous solution of the Usadel equation has its mathematical validity, since the retarded

Green's function is analytical in the upper half of the complex plane. This means that the integral over the energy does not depend on the integration path, so one is free to choose a fitting complex contour $\zeta(E)$. The above substitution therefore corresponds to $\zeta(E) = E + i\delta$ for a small constant δ, which is motivated by the Keldysh contour seen in Fig. 1.1. However, this integration path introduces large numerical errors as the spectrum of Eq. (2.37)

$$\text{spectrum}\, j_x = -\frac{eN_F D}{4\xi_D} \operatorname{Tr}\left(\hat{\tau}^3 \hat{G} \frac{d}{d\xi} \hat{G}\right) \tag{2.38}$$

as a function of E contains δ-function-like peaks, which are difficult to integrate over, shown in Fig. 2.2. A way to broaden the peaks and therefore reach sufficient numerical accuracy without needing an unreasonable number of points is to increase δ. This methods is, however, limited by the distribution function (2.36). The function $\tanh(z)$ has poles for $z_k = i\pi(0.5 + k)$, $k \in \mathbb{Z}$ and although the Keldysh contour may be distorted in the upper half of the complex plane it must still cross the imaginary axis underneath the first pole of $\tanh(z)$ at $z = i\pi/2$. Since the location of the pole depends on temperature the contours discussed above will become invalid for sufficiently small $k_B T$. To have an easier to integrate spectrum as well as a contour beneath the first pole of $\tanh(z)$ the temperature dependent contour

$$\zeta(E) = E + i\left(\frac{\pi k_B T}{2} + 1 - \frac{1}{(1+E^2)^{\frac{3}{2}}}\right) \tag{2.39}$$

is chosen. For every temperature it crosses the imaginary axis in the middle of the origin and the first pole while having a sufficiently large imaginary part away from the imaginary axis. The contour is shown in Fig. 2.3.

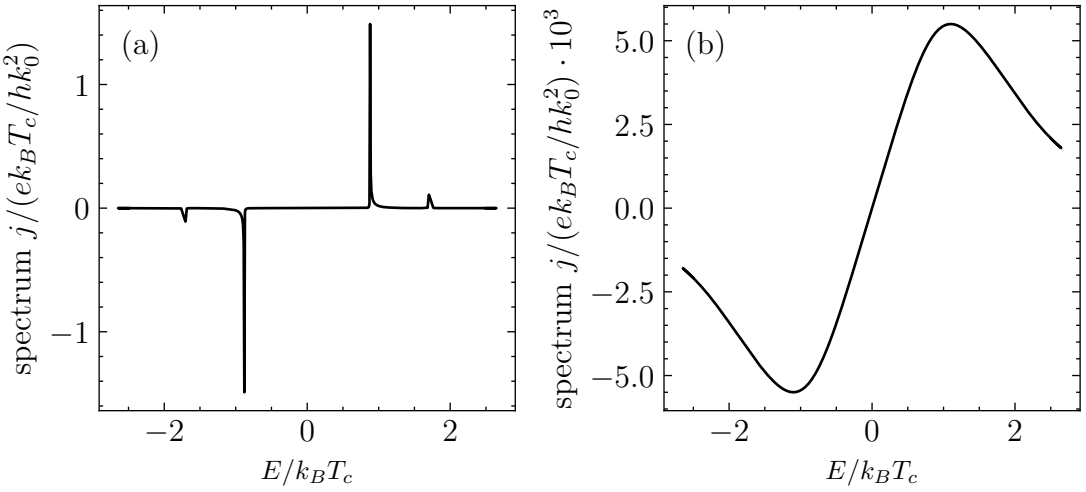

Fig. 2.2 Exemplary depiction of the influence the contour has on the spectrum (2.38) of the current density j from Eq. (2.40). On the left the spectrum was evaluated along the contour $\zeta(E) = E + i\delta$ with $\delta = 10^{-3}$. On the right side it was evaluated along the contour (2.39), with all other relevant parameters staying the same.

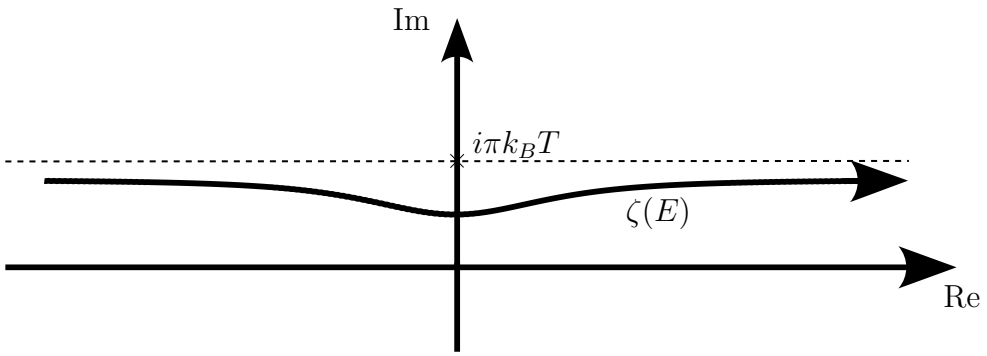

Fig. 2.3 Depiction of the contour $\zeta(E)$ used to evaluate the integral in Eq. (2.40). It always crosses the imaginary axis halfway between the origin and the first pole of $\tanh(z)$. For $E \to \pm\infty$ the contour approaches $1 + \pi k_B T/2$ and is therefore sufficiently far away from the real axis to broaden the peaks of the spectrum as described in the main text.

With the new contour Eq. (2.37) can be transformed to

$$j_x = -\frac{eN_F D}{4\xi_D} \operatorname{Re}\left[\int_{-\infty}^{\infty} \tanh\left(\frac{\zeta(E)}{2k_B T}\right) \operatorname{Tr}\left(\hat{\tau}^3 \hat{G}(\zeta(E)) \frac{d}{d\xi} \hat{G}(\zeta(E))\right) \frac{d\zeta}{dE} dE\right] \tag{2.40}$$

with

$$\frac{d\zeta}{dE} = 1 + i\frac{3E}{(1+E^2)^{\frac{5}{2}}} \tag{2.41}$$

following from the definition of $\zeta(E)$ (2.39).

The code of the numerical implementation can be found at `https://github.com/lKollwitz/bachelor_thesis.git`.

Chapter 3

Results

The spectra as well as phase dependence of the current density of the system will be examined. A closer look will be taken at the critical current densities in dependence of temperature, spin mixing angle and barrier width. At last, the results will be compared to experimental data.

3.1 Spin mixing angle and current density spectra

The current density (2.40) depends on various parameters such as the width and height of the potential barrier for spin up and spin down particles, their energy and momentum parallel to the interface, the temperature of the system and the phase difference between the order parameters on the left and right side of the interface. In order to get comparable results for different polarization strengths suiting quantities for classification are needed. One will be the transmission probabilities $P_T^{\uparrow}$ and $P_T^{\downarrow}$ for spin up ($\uparrow$) and spin down ($\downarrow$) particles. Keeping these probabilities constant ensures a comparable magnitude of the current density for different parameter combinations. The transmission probabilities can be calculated directly from the scattering matrix (2.23) as

$$P_T^{\uparrow,\downarrow} = \left|\Gamma^{\uparrow,\downarrow}\right|^2 \tag{3.1}$$

and are the same for both sides of the interface. The other important quantity that is characterized by the polarization strength is the spin mixing angle θ_{sm} [34]. It describes the difference in phase shifts of the reflected components of the wave functions between spin up and spin down particles. The information about the phase shift is contained in the auxiliary scattering matrix (2.26). The spin mixing angle evaluates to

$$\theta_{sm} = \theta^{\uparrow} - \theta^{\downarrow} = \arg\left(\frac{\Gamma^{\uparrow} r^{\uparrow}}{|\Gamma^{\uparrow} r^{\uparrow}|}\right) - \arg\left(\frac{\Gamma^{\downarrow} r^{\downarrow}}{|\Gamma^{\downarrow} r^{\downarrow}|}\right) \tag{3.2}$$

with $\arg(z) = \theta$ denoting the argument of a complex number $z = re^{i\theta} \in \mathbb{C}$. The transmission probabilities as well as the spin mixing angle depend on the momentum component $k_{\parallel}$ parallel to the interface as shown in Fig. 3.1 for a set of relevant parameters listed in Tab. B.1. In the following, the spin mixing angles used to classify and compare different graphs refer to the quantities at $k_{\parallel} = 0$ if not stated otherwise. The relation between the spin mixing angles at $k_{\parallel} = 0$ seems to hold true for non-zero $k_{\parallel}$ as well, meaning a larger spin mixing angle for particles with momentum parallel to the interface is larger for all possible momentum components parallel to the interface. Though for $k_{\parallel} = k_0$, when no transmission or even penetration into the scattering barrier takes place, θ_{sm} goes to zero regardless of the

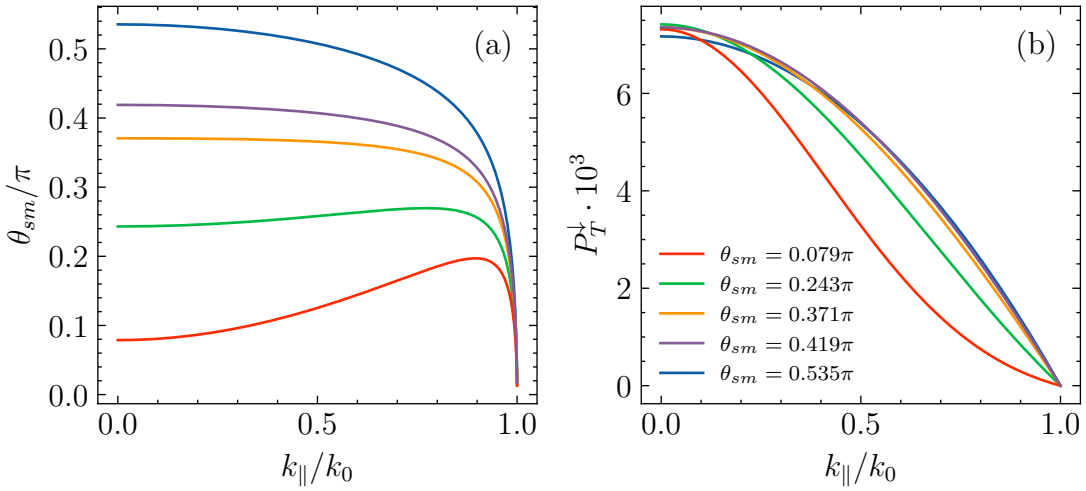

Fig. 3.1 Dependence of the spin mixing angle $\theta_{sm}(k_\parallel)$ as well the transmission probability for spin down ($\downarrow$) electrons $P_T^{\downarrow}$ on the momentum component $k_\parallel$ parallel to the interface. The graphs are classified by their spin mixing angle at $k_\parallel/k_0 = 0$. The relevant parameters were chosen according to Tab. B.1.

chosen parameters. The transmission probabilities all show similar behavior under the change of $k_\parallel$. There is, however, a qualitative change for small spin mixing angles. Here, θ_{sm} increases with larger $k_\parallel$ or lower penetration depth into the barrier. The transmission probability also goes from a concave to a convex shape for large $k_\parallel$ and small θ_{sm}.

With the spin mixing angle as a quantity for parametrization one can take a look at the spectrum of the current density (2.38) for varying phase differences between the superconductors on the left and right side of the interface. These spectra are shown in Fig. 3.2 for the parameters found in Tab. B.1. It can be seen that independent of spin mixing angle the main contributions to the current density come from states with $|E| \leq |\Delta|$ inside the energy gap. These are so called Andreev bound states [34], which similarity in shape to a δ-function lead to the necessity of a different contour integral discussed in Sec. 2.4. Their magnitude and position varies for different φ, with the maximum being reached around $\varphi = \pi/2$. For $\varphi = \pi$ all spectra vanish and there will be no current flowing between the superconductors. For $\varphi > \pi$ the Andreev states are flipped, seen in diagrams (e) and (f) in Fig. 3.2. For larger spin mixing angles the states are broadened but smaller in magnitude with the exception being the one for the smallest spin mixing angle. There, the bound state seems to consist of two overlapping peaks also resulting in a broadened state. There are also contributions to the current density from states with energies very close to the magnitude of the order parameter, which in the case for small spin mixing angles also lie within the energy gap.

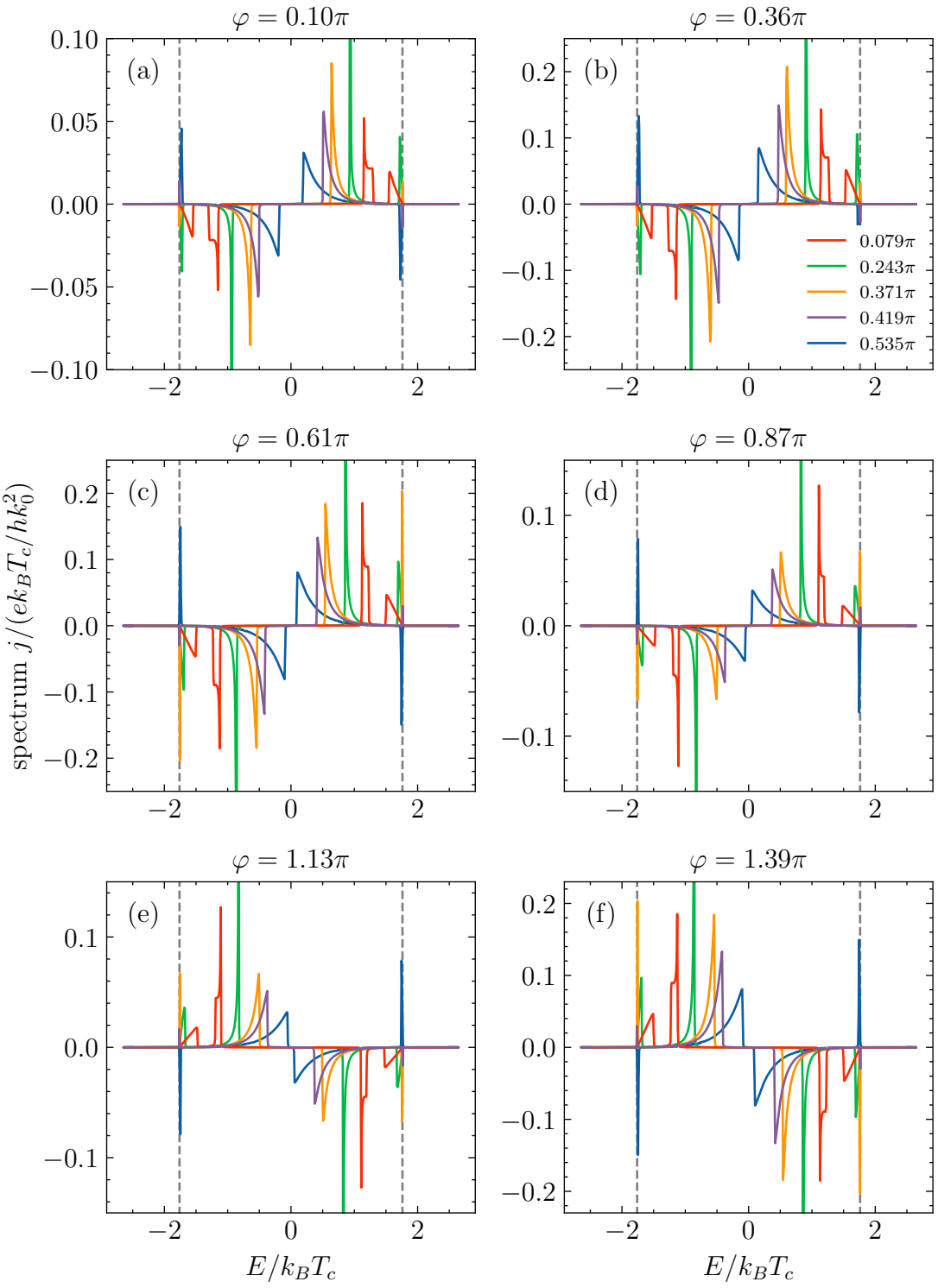

Fig. 3.2 Real part of the spectrum (2.38) of the current density j from Eq. (2.40) evaluated along the contour $\zeta(E) = E + i\delta$ with $\delta = 10^{-3}$ and $T/T_c = 0.2$ for different spin mixing angles θ_{sm} according to the parameters of Tab. B.1. The angle φ is the phase difference of the order parameters with $\Delta \in \mathbb{R}$ and magnitude according to Eq. (1.30) and $\underline{\Delta} = \Delta \exp(i\varphi)$. The vertical lines show the magnitude of the order parameters.

3.2 Critical current dependencies

The examination of the spectrum of the critical current density revealed the existence of Andreev bound states in the system. Integrating the product of the spectrum with the distribution function (2.36) over the energy according to Eq. (2.40) gives the relevant component of the current density $j \equiv j_x$. The Josephson current [12] is caused by the phase difference φ of the superconductors to the left and right of the interface. The dependence on φ is shown for different spin mixing angles and temperatures in Fig. 3.3 with parameters found in Tab. B.1. All graphs are symmetric with respect to the point $(\varphi, j) = (\pi, 0)$ so it was renounced to show the graphs in

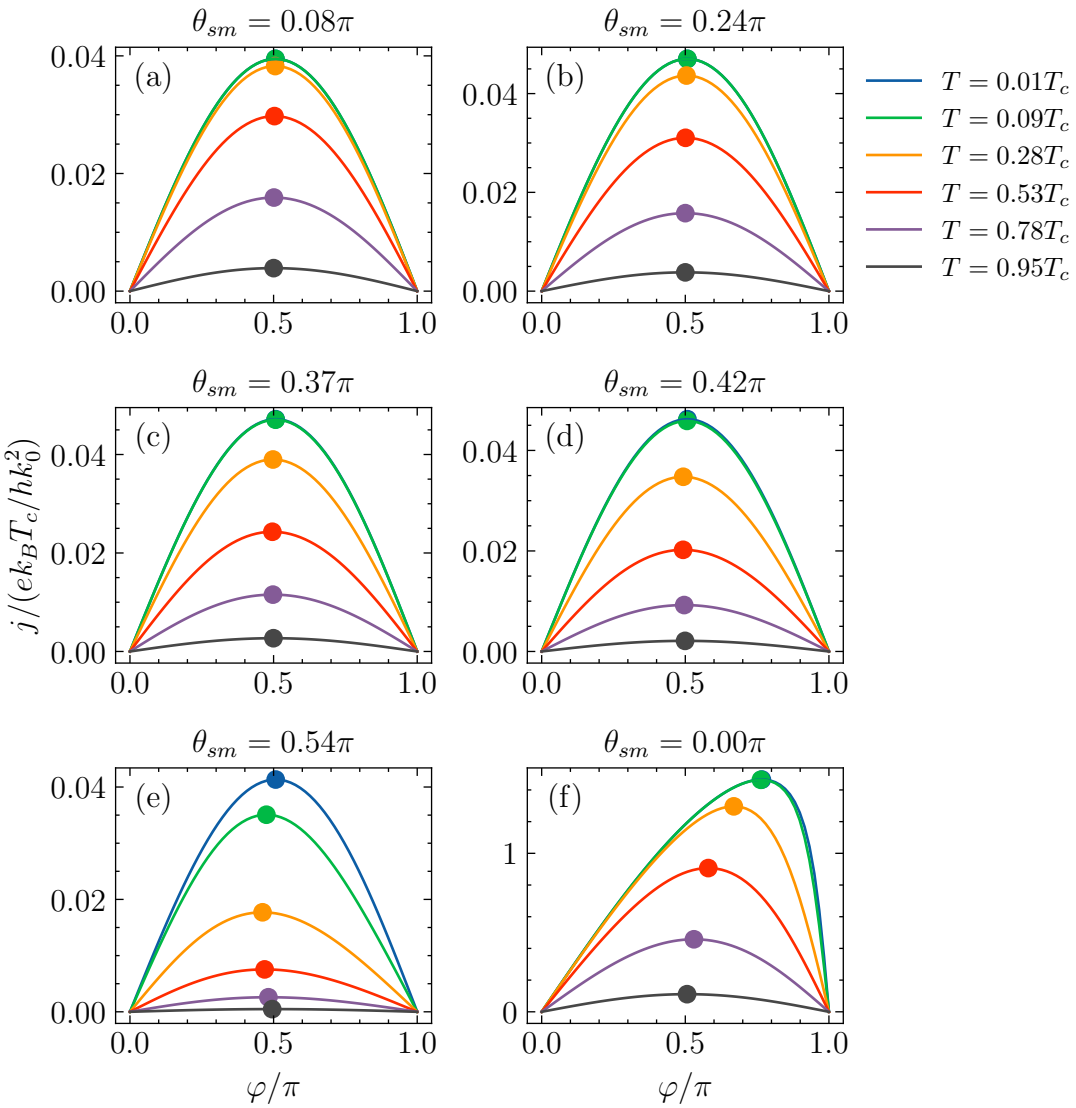

Fig. 3.3 Dependence of the current density j on the phase difference φ of the order parameters Δ and $\underline{\Delta}$ for different temperatures T. Diagrams (a)-(e) correspond to the parameters of Tab. B.1 identified by the spin mixing angle θ_{sm}. Plot (f) shows the behavior for a completely symmetrical system with $(V_1/E_F; V_2^{\uparrow}/E_F; V_2^{\downarrow}/E_F; V_3; \kappa_0^{\uparrow}d^{\uparrow}; \kappa_0^{\downarrow}d^{\downarrow}) = (0; 1.1; 1.1; 0; 0.05; 0.05)$ which results in a high transmission probability of $P_T^{\uparrow} = P_T^{\downarrow} = 0.995$ and a large distortion from a sine wave compared to the graphs of diagrams (a)-(e).

the interval $\varphi \in (\pi, 2\pi]$ to avoid redundancies. It can be seen that all graphs in the diagrams (a)-(e) have a strong resemblance to sine functions as expected from a Josephson junction [35]. The maximum is the so called *critical current density* j_c for the junction, which is realized at the *critical phase difference* φ_c. Due to the junctions having approximately the same transmission probabilities the current densities in the diagrams (a)-(e) all lie in the same range of $j/(ek_BT_c/hk_0^2) \in [0, 0.05]$. This shows only a weak dependence on the magnitude j on the polarization strength of the system, characterized by the spin mixing angle θ_{sm}. The polarization strength does, however, has a large influence on the temperature dependence of j. For the two lowest temperatures the graphs in diagrams (a)-(d) are nearly identical while for diagram (e) they differ a lot. Diagram (f) shows for comparison the critical current density for a completely symmetric junction only differing in the phase of the superconductors. In this case a clear distortion from a pure sine wave can be seen for low temperatures. However, for higher temperatures the graphs again start to resemble the ones in (a)-(e).

A more detailed look at the temperature dependence on the critical current density is shown in Fig. 3.4 with parameters found in Tab. B.1 for diagrams (a) and (c) and in Tab. B.2 for (b) and (d). The second set of parameters has the

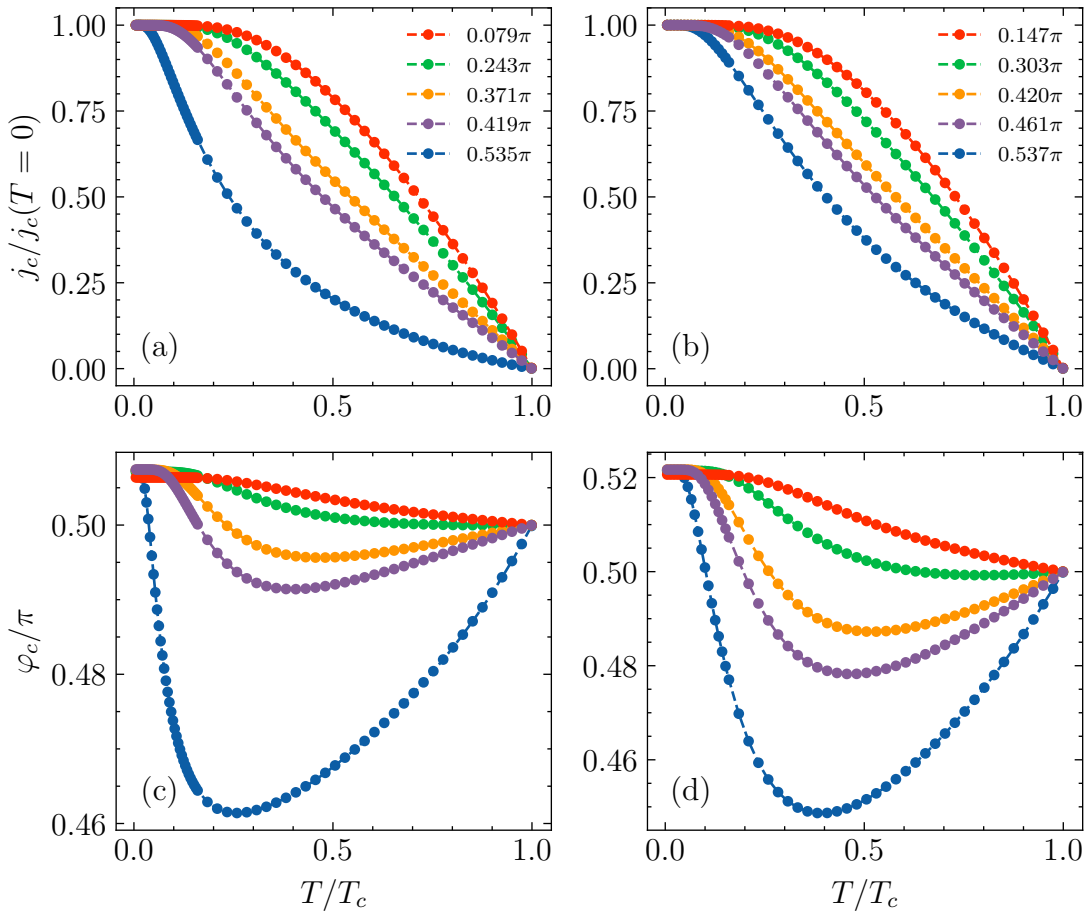

Fig. 3.4 Diagrams (a) and (b) qualitatively show the dependence of the critical current density j_c on temperature T for different spin mixing angles θ_{sm} according to the parameters found in Tab. B.1 for (a) and Tab. B.2 for (b). Diagrams (c) and (d) show the critical phase φ_c at which the critical current density occurs (also see Fig. 3.3). Again for the parameters found in Tab. B.1 for (c) and Tab. B.2 for (d).

same potentials $V_2^{\uparrow}$ as the first but more moderate transmission probabilities of $P_T^{\uparrow} = 0.796$ and $P_T^{\downarrow} \approx 0.103$ compared to the ones for the first set of parameters of $P_T^{\uparrow} = 0.940$ and $P_T^{\downarrow} \approx 7.3 \cdot 10^{-3}$. Diagrams (a) and (b) show the normalized critical current density $j_c/j_c(T=0)$ over the temperature of the system for different spin mixing angles while (c) and (d) show the phase difference φ_c between the superconductors for which the critical current density is realized. A qualitative change from a concave to a convex shape in the temperature region $T/T_c \gtrsim 0.2$ for increasing spin mixing angles can be seen. This was to be expected after considering difference in temperature dependence of the graphs in Fig. 3.3. The phase difference φ_c shows an interesting, non-monotonic behavior for larger spin mixing angles, which seems to closely correlate to the convexity of the graphs in (a) and (b) in the upper temperature region. For the graphs staying convex, φ_c monotonically decreases to $\pi/2$ while for the concave graphs there exist a minimal φ_c below $\pi/2$. For $T \to T_c$ the critical phase φ_c approaches $\pi/2$ for all θ_{sm} in both diagrams (c) and (d). This further highlights the increasing similarity with a pure sine wave with increasing temperature already mentioned in the discussion of Fig. 3.3. The critical phase at low temperatures, shown in more detail in Fig. 3.5, also shows a non-monotonic behavior for increasing spin mixing angles. At first, it seems that $\varphi_c(T/T_c \to 0)$ monotonically increases with increasing θ_{sm}. However, for the largest $\theta_{sm} = 0.535\pi$ a clear decrease can be seen. The slight increase in the graphs for $\theta_{sm} = 0.535\pi$

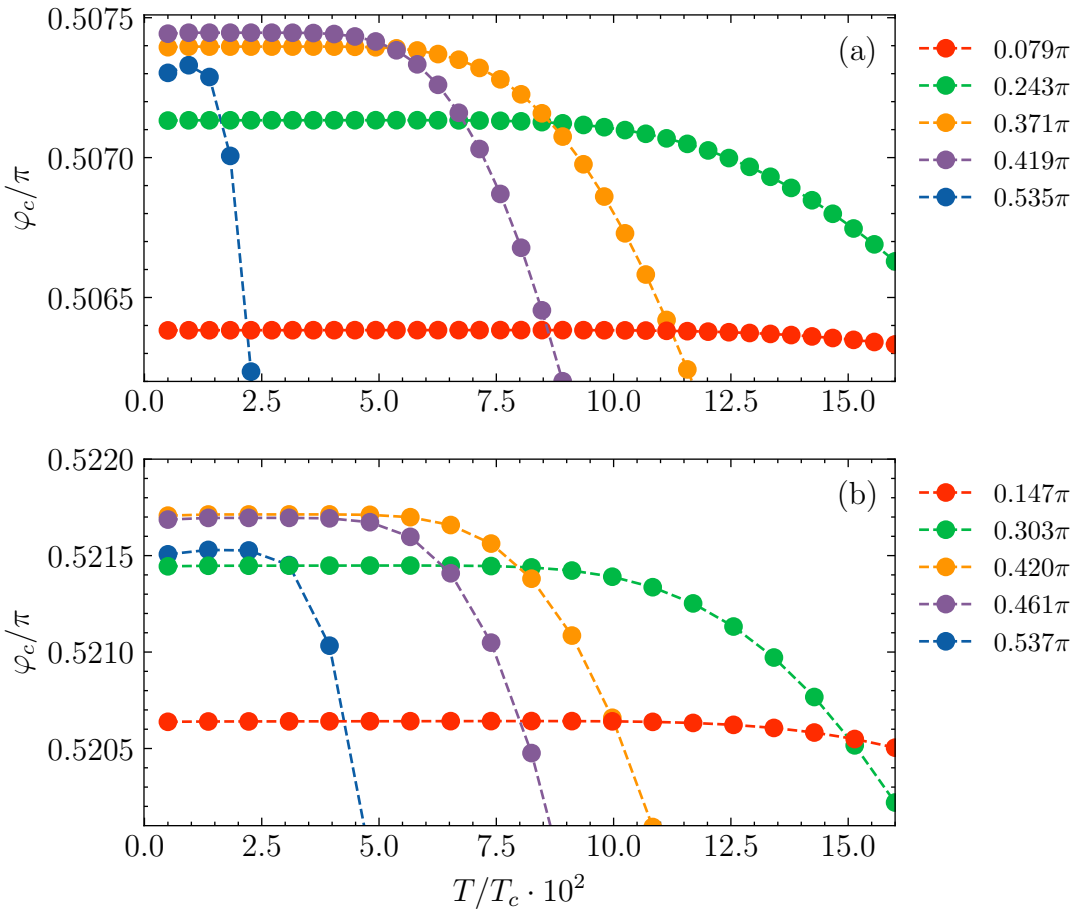

Fig. 3.5 More detailed look on the critical phase difference φ_c for low temperatures T. Diagrams (a) and (b) correspond to (c) and (d) in Fig. 3.4 respectively.

in both (a) and (b) is very likely due to numerical inaccuracies present for low temperatures.

The dependence of the magnitude of the critical current density on the spin mixing angle for different temperatures is shown in Fig. 3.6 for parameters found in Tab. B.1 and Tab. B.2 for diagrams (a) and (b) respectively. One can see that the influence of θ_{sm} on j_c for one particular temperature is rather small compared to the influence of the temperature in general (see Fig. 3.4). Nonetheless, there seems to be a trend towards lower critical current densities for larger spin mixing, seen in both diagrams (a) and (b) across all temperatures. However, this behavior is not monotonic, as for lower temperatures an increase in θ_{sm} also leads to an increase in j_c. Again, the difference in transmission probability between diagrams (a) and (b) does not lead to qualitative changes in the behavior of the system.

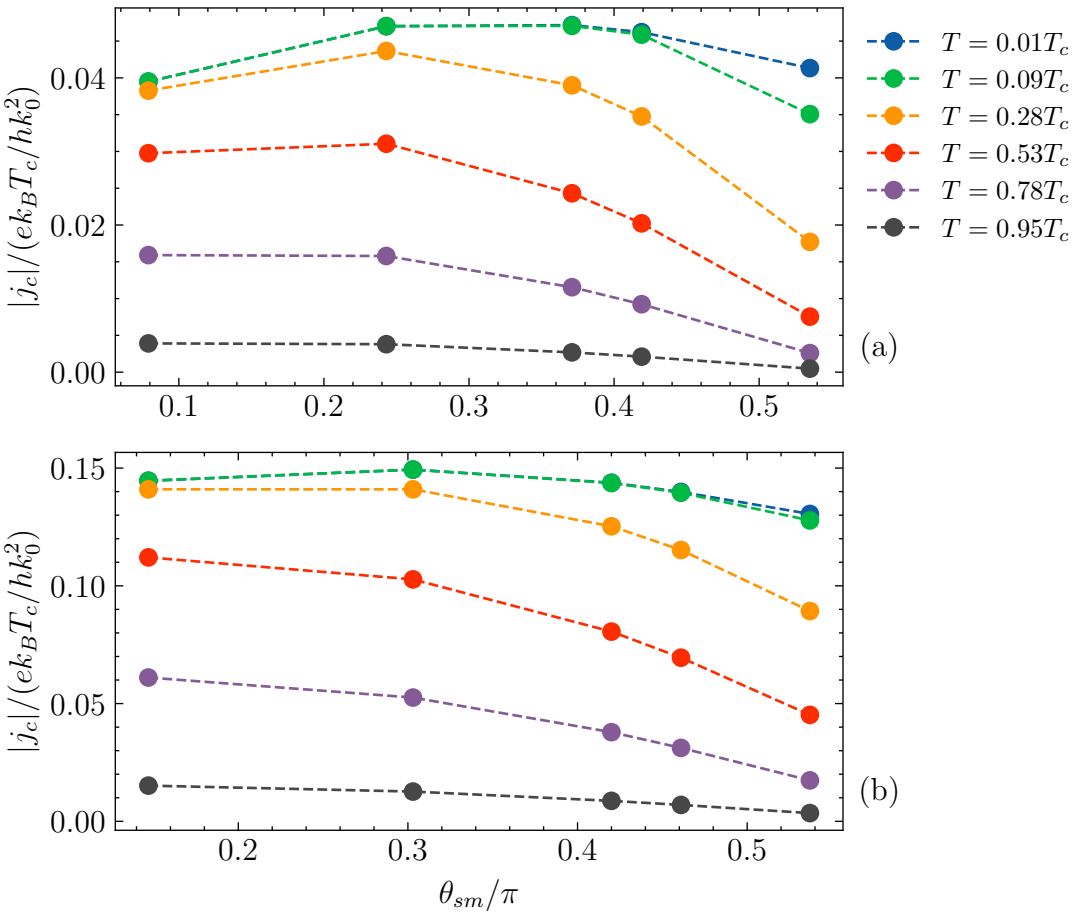

Fig. 3.6 Dependence of the critical current density j_c on the spin mixing angle θ_{sm} for different temperatures T. Diagram (a) shows the values for the parameters found in Tab. B.1 while (b) shows them for the parameters found in Tab. B.2.

At last, the dependence of the thickness of the barrier for different potentials $V_2^{\downarrow}$ on the magnitude of the critical current density will be discussed. The dependence is shown in Fig. 3.7 for the parameters found in Tab. B.1. As the thickness has a non-negligible influence on the spin mixing angle, as can be seen when comparing the ones found in Tab. B.1 with the ones found in Tab. B.2, the height of the potential barrier for spin down particles $V_2^{\downarrow}$ is used for classification. For all potential barrier heights the critical current density falls of exponentially, as one might intuitively

expect, with increase in barrier thickness as seen in diagram (a). This decrease becomes larger for larger $V_2^{\downarrow}$. For very small barrier widths, shown in diagram (b), the critical current density converges towards $|j_c| / (ek_BT_c/hk_0^2) \approx 1.14$ independent of $V_2^{\downarrow}$.

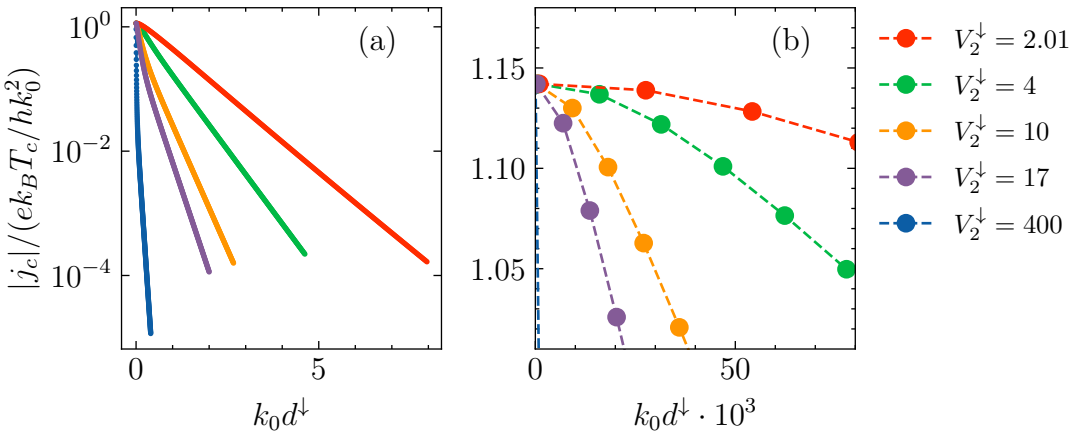

Fig. 3.7 Diagram (a) shows the dependence of the critical current density j_c on the thickness $d^{\downarrow}$ of the potential barrier for spin down ($\downarrow$) particles for different barrier heights $V_2^{\downarrow}$. The parameters are found in Tab. B.1. Diagram (b) shows a more detailed look of the graphs found in (a) for small barrier widths.

3.2.1 Comparison with experiments

The graphs in Fig. 3.4 (a) and (c) agree qualitatively well with experiments [36, 37] for the pure 0- or π-state of the junction. There, the same transition to a convex shape of the graphs for higher temperatures is observed, while still being concave for lower ones. However, there also exists a phase transition between these two states found for some barrier widths [37, 38]. This has the effect of the critical current density going to zeros and then increasing again before going back to zero, shown in [37, Fig. 2]. This sadly could not have been produced in this model. The reason from this, apart still existing errors in the numerical implementation, which can be fully ruled out, might be an unfitting parameter set. There were of course many more parameter configurations that have been tested but none resulting in this phase transition were found. For the specific case of a rectangular potential barrier the 0-π-state phase transition described above cannot alone describe the observed behavior of the critical current [39]. It still exists an increase for increasing temperature but the current density does not drop to zero. However, this behavior also could not have been reproduced in this thesis. Yet another reason might be the model itself. It has turned out quite difficult to produce spin mixing angles significantly larger than $\theta_{sm} = \pi/2$. The reason for this may lie in the shape of the potential barrier. The rectangular shape allows for an analytical computation of the scattering matrix, but has the drawback of not having regions right beside the barrier where spin mixing angle can be accumulated before the scattering. This could be fixed by introducing a small potential step for one spin direction, which is still below the Fermi energy. Another way might be to change the scattering potential to a trapezoidal shape, again with different heights and widths for both spin directions. Another measurable effect that sadly could not have been observed

in the simulation is the increase of the magnitude of the critical current density with increasing barrier width, as observed in the experiment done in [38]. Again, this is caused by a phase transition from the 0- to the π-state of the junction. Therefore, the same reasons as above as to why it could not have been seen in this model apply here as well.

Conclusion

In this thesis, the main ideas of the quasi-classical theory of superconductivity were outlined with focus on the diffuse limit. The Usadel equation (1.26) for the isotropic Green's function $\check{G}$ was derived. The main difficulty in describing superconducting hybrid structures, that of the formulation of boundary conditions, was approached via a scattering matrix formulation that allowed the connection of the ballistic propagator $\hat{g}$ near the interface with the isotropic Green's function $\hat{G}$ in the bulk of the superconductor by using the conservation of the matrix current $\hat{\mathcal{I}}$. This allowed for a direct calculation of the current density j_c of the junction without the need to explicitly solve the Usadel equation. Numerical calculations were done in order to investigate the dependence of j_c on various relevant parameters. The dependence of j_c on the temperature was in qualitative agreement with experiment for cases without a phase transition happening in the junction. The phase transition itself could not have been reproduced. In order to find the reason for that further investigation will be required that was beyond the scope of this thesis. This may include the calculation for different barrier shapes as was done in [40] or test different parameter configurations. Further, it may be that the diffusive description suppresses the effect that leads to the behavior of the current density observed in [39]. Therefore, a ballistic treatment of the system might be appropriate. An interesting phenomenon that was produced with the methods above and which no prior literature, to the best of my knowledge, seems to address was found in the dependence of the critical phase φ_c, which for strong polarization shows a non-monotonic dependence on temperature.

The scattering matrix approach together with the methods discussed in Sec. 2.4 could be implemented easily in a straight forward manner and resulted in reasonable fast computation times. The implementation proved to be quite stable with the main reason for unsuccessful runs being the numerical inversion of matrices that were singular to machine precision. This however only happened in cases for very low transmissions $P_T \lesssim 10^{-40}$. For reasonable parameters like the ones used above this problem never occurred. The scattering matrix approach is therefore very suitable for numerical calculations of superconducting hybrid structure in the diffusive limit. The work in this thesis incorporated spin dependent effects with trivial structure in channel space but since the approach can be readily generalized to incorporate arbitrary numbers of scattering channels this thesis as well as the numerical implementation may be used as a starting point for the investigation of more complex systems.

Appendix A

Calculations

A.1 Polar decomposition of the scattering matrix

The general scattering matrix

$$\hat{\mathbf{S}} = \begin{pmatrix} R & \underline{T} \\ T & -\underline{R} \end{pmatrix} \tag{A.1}$$

with dimensions $n \times n$ for R, $m \times m$ for $\underline{R}$, $n \times m$ for $\underline{T}$ and $m \times n$ for T is considered. One can perform a polar decomposition by writing, for example, the matrix R as

$$R = \left(RR^\dagger\right)^{\frac{1}{2}} \left(RR^\dagger\right)^{-\frac{1}{2}} R \tag{A.2}$$

$$= PU \tag{A.3}$$

$$\text{with} \quad P = \left(RR^\dagger\right)^{\frac{1}{2}} \quad \text{and} \quad U = \left(RR^\dagger\right)^{-\frac{1}{2}} R\,. \tag{A.4}$$

It can be seen that

$$P^\dagger = \left[\left(RR^\dagger\right)^{\frac{1}{2}}\right]^\dagger = \left[\left(RR^\dagger\right)^\dagger\right]^{\frac{1}{2}} \tag{A.5}$$

$$= \left(RR^\dagger\right)^{\frac{1}{2}} = P \tag{A.6}$$

$$\tag{A.7}$$

and

$$U^\dagger = \left[\left(RR^\dagger\right)^{-\frac{1}{2}} R\right]^\dagger = R^\dagger \left(RR^\dagger\right)^{-\frac{1}{2}} \tag{A.8}$$

$$= R^{-1} RR^\dagger \left(RR^\dagger\right)^{-\frac{1}{2}} = R^{-1} \left(RR^\dagger\right)^{\frac{1}{2}} \tag{A.9}$$

$$= \left[\left(RR^\dagger\right)^{-\frac{1}{2}} R\right]^{-1} = U^{-1}\,, \tag{A.10}$$

so P is hermitian and U is unitary.

A.2 Equivalence of equations (1.52a)-(1.52d)

From the normalization condition (1.27) follows $\hat{G} \cdot \hat{G} = \hat{1}$ for the retarded part of the isotropic Green's function. With the unitary property of $\hat{\mathcal{S}}$ it follows that

$$\hat{G}_1 \cdot \hat{G}_1 = \hat{1}\,, \qquad \hat{G}_2 \cdot \hat{G}_2 = \hat{1}\,. \tag{A.11}$$

First, the equivalence between Eqs. (1.52a) and (1.52b) is shown by

$$\Rightarrow \quad \hat{G}_2 + \hat{G}_1 = \hat{G}_1 + \hat{G}_2 \tag{A.12}$$

$$\overset{(A.11)}{\Rightarrow} \quad \hat{G}_2 + \hat{G}_2\hat{G}_2\hat{G}_1 = \hat{G}_1 + \hat{G}_2\hat{G}_1\hat{G}_1 \tag{A.13}$$

$$\Rightarrow \quad \hat{G}_2\left(\hat{1} + \hat{G}_2\hat{G}_1\right) = \left(\hat{1} + \hat{G}_2\hat{G}_1\right)\hat{G}_1 \tag{A.14}$$

$$\Rightarrow \quad \left(\hat{1} + \hat{G}_2\hat{G}_1\right)^{-1}\hat{G}_2 = \hat{G}_1\left(\hat{1} + \hat{G}_2\hat{G}_1\right)^{-1} \tag{A.15}$$

$$\Rightarrow \quad \left(\hat{1} + \hat{G}_2\hat{G}_1\right)^{-1}\hat{G}_2 + \left(\hat{1} + \hat{G}_2\hat{G}_1\right)^{-1} = \hat{G}_1\left(\hat{1} + \hat{G}_2\hat{G}_1\right)^{-1} + \left(\hat{1} + \hat{G}_2\hat{G}_1\right)^{-1} \tag{A.16}$$

$$\Rightarrow \quad \left(\hat{1} + \hat{G}_2\hat{G}_1\right)^{-1}\left(\hat{G}_2 + \hat{1}\right) = \left(\hat{G}_1 + \hat{1}\right)\left(\hat{1} + \hat{G}_2\hat{G}_1\right)^{-1} \tag{A.17}$$

$$\Rightarrow \quad 2\left(\hat{1} + \hat{G}_2\hat{G}_1\right)^{-1}\left(\hat{G}_2 + \hat{1}\right) - \hat{1} = 2\left(\hat{G}_1 + \hat{1}\right)\left(\hat{1} + \hat{G}_2\hat{G}_1\right)^{-1} - \hat{1}\,. \tag{A.18}$$

Similarly, the equivalence between Eqs. (1.52c) and (1.52d) is shown by

$$\Rightarrow \quad \hat{G}_2 + \hat{G}_1 = \hat{G}_1 + \hat{G}_2 \tag{A.19}$$

$$\overset{(A.11)}{\Rightarrow} \quad \hat{G}_2 + \hat{G}_1\hat{G}_2\hat{G}_2 = \hat{G}_1 + \hat{G}_1\hat{G}_1\hat{G}_2 \tag{A.20}$$

$$\Rightarrow \quad \left(\hat{1} + \hat{G}_1\hat{G}_2\right)\hat{G}_2 = \hat{G}_1\left(\hat{1} + \hat{G}_1\hat{G}_2\right) \tag{A.21}$$

$$\Rightarrow \quad \left(\hat{1} + \hat{G}_1\hat{G}_2\right)\hat{G}_2 - \left(\hat{1} + \hat{G}_1\hat{G}_2\right) = \hat{G}_1\left(\hat{1} + \hat{G}_1\hat{G}_2\right) - \left(\hat{1} + \hat{G}_1\hat{G}_2\right) \tag{A.22}$$

$$\Rightarrow \quad \left(\hat{1} + \hat{G}_1\hat{G}_2\right)\left(\hat{G}_2 - \hat{1}\right) = \left(\hat{G}_1 - \hat{1}\right)\left(\hat{1} + \hat{G}_1\hat{G}_2\right) \tag{A.23}$$

$$\Rightarrow \quad \left(\hat{G}_2 - \hat{1}\right)\left(\hat{1} + \hat{G}_1\hat{G}_2\right)^{-1} = \left(\hat{1} + \hat{G}_1\hat{G}_2\right)^{-1}\left(\hat{G}_1 - \hat{1}\right) \tag{A.24}$$

$$\Rightarrow \quad 2\left(\hat{G}_2 - \hat{1}\right)\left(\hat{1} + \hat{G}_1\hat{G}_2\right)^{-1} + \hat{1} = 2\left(\hat{1} + \hat{G}_1\hat{G}_2\right)^{-1}\left(\hat{G}_1 - \hat{1}\right) + \hat{1}\,. \tag{A.25}$$

Lastly, the equivalence between Eqs. (1.52a) and (1.52c) is shown by

$$\Rightarrow \quad 2\hat{1} + \hat{G}_1\hat{G}_2 + \hat{G}_2\hat{G}_1 = 2\hat{1} + \hat{G}_1\hat{G}_2 + \hat{G}_2\hat{G}_1 \tag{A.26}$$

$$\overset{(A.11)}{\Rightarrow} \quad 2\hat{1} + \hat{G}_1\hat{G}_2 + \hat{G}_2\hat{G}_1 = \hat{1} + \hat{G}_1\hat{G}_2 + \hat{G}_2\hat{G}_1 + \hat{G}_2\hat{G}_1\hat{G}_1\hat{G}_2 \tag{A.27}$$

$$\Rightarrow \quad \hat{1} + \hat{G}_1\hat{G}_2 + \hat{1} + \hat{G}_2\hat{G}_1 = \left(\hat{1} + \hat{G}_2\hat{G}_1\right)\left(\hat{1} + \hat{G}_1\hat{G}_2\right) \tag{A.28}$$

$$\Rightarrow \quad \left(\hat{1} + \hat{G}_2\hat{G}_1\right)^{-1} = \hat{1} - \left(\hat{1} + \hat{G}_1\hat{G}_2\right)^{-1} \tag{A.29}$$

$$\overset{(A.15)}{\Rightarrow} \left(\hat{1} + \hat{G}_2\hat{G}_1\right)^{-1}\hat{G}_2 + \left(\hat{1} + \hat{G}_2\hat{G}_1\right)^{-1} = \hat{G}_1\left(\hat{1} + \hat{G}_2\hat{G}_1\right)^{-1} - \left(\hat{1} + \hat{G}_1\hat{G}_2\right)^{-1} + \hat{1} \tag{A.30}$$

$$\Rightarrow \quad \left(\hat{1} + \hat{G}_2\hat{G}_1\right)^{-1}\left(\hat{G}_2 + \hat{1}\right) = \left(\hat{1} + \hat{G}_1\hat{G}_2\right)^{-1}\hat{G}_1 - \left(\hat{1} + \hat{G}_1\hat{G}_2\right)^{-1} + \hat{1} \tag{A.31}$$

$$\Rightarrow \quad 2\left(\hat{1} + \hat{G}_2\hat{G}_1\right)^{-1}\left(\hat{G}_2 + \hat{1}\right) - \hat{1} = 2\left(\hat{1} + \hat{G}_1\hat{G}_2\right)^{-1}\left(\hat{G}_1 - \hat{1}\right) + \hat{1}\,. \tag{A.32}$$

A.3 Solution for the reflection and transmission coefficient

Starting with the system of equations

$$\begin{pmatrix} -1 & \alpha c - i\beta s \\ 1 & \alpha^{-1}c - (i\beta)^{-1}s \end{pmatrix} \cdot \begin{pmatrix} R \\ T \end{pmatrix} = \begin{pmatrix} 1 \\ 1 \end{pmatrix} \tag{A.33}$$

for the reflection and transmission amplitude one can multiply from the right with the inverse of the matrix to obtain

$$\begin{pmatrix} R \\ T \end{pmatrix} = \frac{1}{-\left(\alpha^{-1}c - (i\beta)^{-1}s\right) - \alpha c + i\beta s} \begin{pmatrix} \alpha^{-1}c - (i\beta)^{-1}s & -\alpha c + i\beta s \\ -1 & -1 \end{pmatrix} \begin{pmatrix} 1 \\ 1 \end{pmatrix} \tag{A.34}$$

$$= -\frac{1}{\left(\alpha + \alpha^{-1}\right)c - i\left(\beta - \beta^{-1}\right)s} \begin{pmatrix} \alpha^{-1}c - (i\beta)^{-1}s - \alpha c + i\beta s \\ -2 \end{pmatrix} \tag{A.35}$$

$$= \frac{1}{\left(\alpha + \alpha^{-1}\right)c - i\left(\beta - \beta^{-1}\right)s} \begin{pmatrix} \left(\alpha - \alpha^{-1}\right)c - i\left(\beta + \beta^{-1}\right)s \\ 2 \end{pmatrix}, \tag{A.36}$$

with the inverse of a 2×2-matrix being

$$\begin{pmatrix} a & b \\ c & d \end{pmatrix}^{-1} = \frac{1}{ad - bc} \begin{pmatrix} d & -b \\ -c & a \end{pmatrix}. \tag{A.37}$$

A.4 Keldysh component for the current density

With the relations (1.29) it follows with $\hat{G}^R = \hat{G}$ that

$$\left[\check{G} \cdot \nabla\check{G}\right]^K = \hat{G}^R \cdot \nabla\hat{G}^K + \hat{G}^K \cdot \nabla\hat{G}^A \tag{A.38}$$

$$= \tanh\left(\frac{E}{2k_BT}\right)\left[G^R \cdot \nabla\left(\hat{G}^R - \hat{G}^A\right) + \left(\hat{G}^R - \hat{G}^A\right) \cdot \nabla\hat{G}^A\right] \tag{A.39}$$

$$= \tanh\left(\frac{E}{2k_BT}\right)\left[\hat{G}^R \cdot \nabla\hat{G}^R - \hat{G}^R \cdot \nabla\hat{G}^A + \hat{G}^R \cdot \nabla\hat{G}^A - \hat{G}^A \cdot \nabla\hat{G}^A\right] \tag{A.40}$$

$$= \tanh\left(\frac{E}{2k_BT}\right)\left[\hat{G}^R \cdot \nabla\hat{G}^R - \hat{G}^A \cdot \nabla\hat{G}^A\right] \tag{A.41}$$

$$= \tanh\left(\frac{E}{2k_BT}\right)\left[\hat{G}^R \cdot \nabla\hat{G}^R - \hat{\tau}_3\left(\hat{G}^R\right)^\dagger\hat{\tau}_3 \cdot \nabla\left(\hat{\tau}_3\left(\hat{G}^R\right)^\dagger\hat{\tau}_3\right)\right] \tag{A.42}$$

$$= \tanh\left(\frac{E}{2k_BT}\right)\left[\hat{G}^R \cdot \nabla\hat{G}^R - \hat{\tau}_3\left(\nabla\hat{G}^R \cdot \hat{G}^R\right)^\dagger\hat{\tau}_3\right] \tag{A.43}$$

$$= \tanh\left(\frac{E}{2k_BT}\right)\left[\hat{G}^R \cdot \nabla\hat{G}^R + \hat{\tau}_3\left(\hat{G}^R \cdot \nabla\hat{G}^R\right)^\dagger\hat{\tau}_3\right] \tag{A.44}$$

$$= \tanh\left(\frac{E}{2k_BT}\right)\left[\hat{G} \cdot \nabla\hat{G} + \hat{\tau}_3\left(\hat{G} \cdot \nabla\hat{G}\right)^\dagger\hat{\tau}_3\right]. \tag{A.45}$$

In the second to last line the relation

$$\hat{G} \cdot \hat{G} = \hat{1} \tag{A.46}$$

$$\Rightarrow \quad \nabla \left(\hat{G} \cdot \hat{G} \right) = \hat{0} \tag{A.47}$$

$$\Rightarrow \quad \nabla \hat{G} \cdot \hat{G} + \hat{G} \cdot \nabla \hat{G} = \hat{0} \tag{A.48}$$

$$\Rightarrow \quad \nabla \hat{G} \cdot \hat{G} = -\hat{G} \cdot \nabla \hat{G} \tag{A.49}$$

following from the normalization of $\hat{G}$ was used.

Appendix B

Tables

Tab. B.1 Parameter set for different polarization strengths. The parameters $(V_1/E_F, V_3/E_F, V_2^{\uparrow}/E_F, \kappa_0^{\uparrow}d^{\uparrow},) = (0, 0, 1.01, 0.05)$ stayed constant. This configuration resulted in a high transmission for spin up ($\uparrow$) particles of $P_T^{\uparrow}(k_{\parallel} = 0) = 0.940$. The width $\kappa_0^{\downarrow}d^{\downarrow}$ was chosen in a way to keep $P_T^{\downarrow}(k_{\parallel} = 0)$ approximately constant.

$V_2^{\downarrow}/E_F$	$\kappa_0^{\downarrow}d^{\downarrow}$	$\theta_{sm}(k_{\parallel} = 0)/\pi$	$P_T^{\downarrow}(k_{\parallel} = 0) \cdot 10^3$
2.01	3.15	0.079	7.3
4.00	3.00	0.243	7.4
10.00	2.64	0.371	7.4
17.00	2.40	0.419	7.4
400.00	1.00	0.535	7.2

Tab. B.2 Parameter set for different polarization strengths. The parameters $(V_1/E_F, V_3/E_F, V_2^{\uparrow}/E_F, \kappa_0^{\uparrow}d^{\uparrow},) = (0, 0, 1.01, 0.1)$ stayed constant. This configuration resulted in a high transmission for spin up ($\uparrow$) particles of $P_T^{\uparrow}(k_{\parallel} = 0) = 0.796$. The width $\kappa_0^{\downarrow}d^{\downarrow}$ was chosen in a way to keep $P_T^{\downarrow}(k_{\parallel} = 0)$ approximately constant.

$V_2^{\downarrow}/E_F$	$\kappa_0^{\downarrow}d^{\downarrow}$	$\theta_{sm}(k_{\parallel} = 0)/\pi$	$P_T^{\downarrow}(k_{\parallel} = 0)$
2.01	1.801	0.147	0.103
4.00	1.670	0.303	0.103
10.00	1.335	0.420	0.103
17.00	1.130	0.461	0.103
400.00	0.290	0.537	0.103

Bibliography

[1] K. D. Usadel. “Generalized diffusion equation for superconducting alloys”. In: *Physical Review Letters* 25.8 (1970), p. 507.

[2] H. Kamerlingh Onnes. “Further experiments with liquid helium. C. On the change of electric resistance of pure metals at very low temperatures etc. IV. The resistance of pure mercury at helium temperatures”. In: *Through Measurement to Knowledge*. Springer, 1991, pp. 261–263.

[3] F. London and H. London. “The Electromagnetic Equations of the Supraconductor”. In: *Proceedings of the Royal Society of London Series A* 149.866 (Mar. 1935), pp. 71–88. DOI: 10.1098/rspa.1935.0048.

[4] V. L. Ginzburg and L. D. Landau. “On the Theory of superconductivity”. In: *Zh. Eksp. Teor. Fiz.* 20 (1950), pp. 1064–1082.

[5] J. Bardeen, L. N. Cooper, and J. R. Schrieffer. “Theory of Superconductivity”. In: *Phys. Rev.* 108.5 (1957), p. 1175.

[6] L. P. Gor’kov. “On the energy spectrum of superconductors”. In: *Sov. Phys. JETP* 34.3 (1958), p. 505.

[7] G. Eilenberger. “Transformation of Gorkov’s equation for type II superconductors into transport-like equations”. In: *Zeitschrift für Physik A Hadrons and nuclei* 214.2 (1968), pp. 195–213.

[8] A. I. Larkin and Y. N. Ovchinnikov. “Quasiclassical method in the theory of superconductivity”. In: *Sov Phys JETP* 28.6 (1969), pp. 1200–1205.

[9] H. Meissner. “Superconductivity of contacts with interposed barriers”. In: *Physical Review* 117.3 (1960), p. 672.

[10] A. F. Andreev. “The thermal conductivity of the intermediate state in superconductors”. In: *Журнал экспериментальной и теоретической физики* 46.5 (1964), pp. 1823–1828.

[11] P. G. De Gennes and D. Saint-James. “Elementary excitations in the vicinity of a normal metal-superconducting metal contact”. In: *Phys. Letters* 4 (1963).

[12] B. D. Josephson. “Possible new effects in superconductive tunnelling”. In: *Physics letters* 1.7 (1962), pp. 251–253.

[13] M. Eschrig et al. “Singlet-triplet mixing in superconductor-ferromagnet hybrid devices”. In: *Advances in Solid State Physics*. Springer, 2004, pp. 533–545.

[14] V. L. Berezinskii. “New model of the anisotropic phase of superfluid He3”. In: *Jetp Lett* 20.9 (1974), pp. 287–289.

[15] J. Linder and J. W. A. Robinson. “Superconducting spintronics”. In: *Nature Physics* 11.4 (2015), pp. 307–315.

[16] W. L. McMillan. “Tunneling model of the superconducting proximity effect”. In: *Physical Review* 175.2 (1968), p. 537.

[17] A. V. Zaitsev. "Quasiclassical equations of the theory of superconductivity for contiguous metals and the properties of constricted microcontacts". In: *Zh. Eksp. Teor. Fiz* 86 (1984), pp. 1742–1758.

[18] A. Millis, D. Rainer, and J. A. Sauls. "Quasiclassical theory of superconductivity near magnetically active interfaces". In: *Physical Review B* 38.7 (1988), p. 4504.

[19] M. Eschrig. "Distribution functions in nonequilibrium theory of superconductivity and Andreev spectroscopy in unconventional superconductors". In: *Physical Review B* 61.13 (2000), p. 9061.

[20] E. Zhao, T. Löfwander, and J. A. Sauls. "Nonequilibrium superconductivity near spin-active interfaces". In: *Physical Review B* 70.13 (2004), p. 134510.

[21] M. Eschrig. "Scattering problem in nonequilibrium quasiclassical theory of metals and superconductors: general boundary conditions and applications". In: *Physical Review B* 80.13 (2009), p. 134511.

[22] A. Cottet et al. "Spin-dependent boundary conditions for isotropic superconducting Green's functions". In: *Phys. Rev. B* 80 (18 2009), p. 184511.

[23] M. Eschrig et al. "General boundary conditions for quasiclassical theory of superconductivity in the diffusive limit: application to strongly spin-polarized systems". In: *New Journal of Physics* 17.8 (2015), p. 083037.

[24] L. V. Keldysh. "Diagram technique for nonequilibrium processes". In: *Sov. Phys. JETP* 20.4 (1965), pp. 1018–1026.

[25] J. Rammer and H. Smith. "Quantum field-theoretical methods in transport theory of metals". In: *Reviews of modern physics* 58.2 (1986), p. 323.

[26] K. H. Bennemann and J. B. Ketterson. *The Physics of Superconductors*. Vol. 2. Springer, 2004.

[27] L. P. Gor'kov. "Microscopic derivation of the Ginzburg-Landau equations in the theory of superconductivity". In: *Sov. Phys. JETP* 9.6 (1959), pp. 1364–1367.

[28] L. P. Gor'kov. "Theory of superconducting alloys in a strong magnetic field near the critical temperature". In: *Soviet Physics JETP* 10 (1960), p. 998.

[29] F. Gross et al. "Anomalous temperature dependence of the magnetic field penetration depth in superconducting UBe13". In: *Zeitschrift für Physik B Condensed Matter* 64.2 (1986), pp. 175–188.

[30] K. Senapati, Mark G. Blamire, and Z. H. Barber. "Spin-filter Josephson junctions". In: *Nature materials* 10.11 (2011), pp. 849–852.

[31] Y. V. Nazarov. "Novel circuit theory of Andreev reflection". In: *Superlattices and microstructures* 25.5-6 (1999), pp. 1221–1231.

[32] J. Kopu et al. "Transfer-matrix description of heterostructures involving superconductors and ferromagnets". In: *Physical Review B* 69.9 (2004), p. 094501.

[33] Y. V. Nazarov. "Circuit theory of Andreev conductance". In: *Physical review letters* 73.10 (1994), p. 1420.

[34] M. Eschrig. "Spin-polarized supercurrents for spintronics: a review of current progress". In: *Reports on Progress in Physics* 78.10 (2015), p. 104501.

[35] A. A. Golubov, M .Y. Kupriyanov, and E. Il'Ichev. "The current-phase relation in Josephson junctions". In: *Reviews of modern physics* 76.2 (2004), p. 411.

[36] T. Kontos et al. "Josephson junction through a thin ferromagnetic layer: negative coupling". In: *Physical review letters* 89.13 (2002), p. 137007.

[37] V. A. Oboznov et al. "Thickness dependence of the Josephson ground states of superconductor-ferromagnet-superconductor junctions". In: *Physical review letters* 96.19 (2006), p. 197003.

[38] T. S. Khaire, W. P. Pratt Jr., and N. O. Birge. "Critical current behavior in Josephson junctions with the weak ferromagnet PdNi". In: *Physical Review B* 79.9 (2009), p. 094523.

[39] R. Caruso et al. "Tuning of magnetic activity in spin-filter Josephson junctions towards spin-triplet transport". In: *Physical Review Letters* 122.4 (2019), p. 047002.

[40] R. Grein et al. "Theory of superconductor-ferromagnet point-contact spectra: The case of strong spin polarization". In: *Physical Review B* 81.9 (2010), p. 094508.

Acknowledgment

First and foremost I want to thank Prof. Dr. Eschrig for his extensive supervision and explanations, without this thesis would not have been possible to create. I also want to thank Anna Levbarg for helpful comments and discussions. Further, I want to thank my girlfriend, who took on a lot of responsibilities outside my studies in order for me to focus on this thesis and helped me get through the times, when nothing seemed to work. Lastly, I want to thank my parents, who supported me financially and always had a friendly ear.